

# OF OCEAN WAVES AND SEA ICE<sup>1</sup>

*Vernon A. Squire*

Department of Mathematics and Statistics, University of Otago, Dunedin,  
New Zealand

*John P. Dugan*

ONR European Office, 223 Old Marylebone Road, London NW1 5TH,  
United Kingdom

*Peter Wadhams*

Scott Polar Research Institute, Lensfield Road, Cambridge CB2 1ER,  
United Kingdom

*Philip J. Rottier*

BAeSEMA Limited, 1 Atlantic Quay, Broomielaw, Glasgow G2 8JE,  
United Kingdom

*Antony K. Liu*

Oceans and Ice Branch, NASA Goddard Space Flight Center, Greenbelt,  
Maryland 20771

KEY WORDS: marginal ice zone, continuous sea ice, bipolar, modeling, field  
experiments

---

<sup>1</sup> The US Government has the right to retain a nonexclusive, royalty-free license in and to any copyright covering this paper.

## 1. INTRODUCTION

The global geophysical role of wave-ice interaction has two facets: the physical effects of waves on an ice cover or of the ice on the waves; and the use of waves as a diagnostic tool in ice mechanics. The physical effects include the ability of waves to break up ice sheets into floes and to herd these floes into patterns that determine the morphology of the marginal ice zone, the break-up of tabular icebergs, the calving of ice tongues, and the generation of ambient noise. The diagnostic role stems from the long-range propagation of wave energy in the form of flexural-gravity waves through ice sheets, and the information that the dispersion relation and attenuation rates can give us about ice properties and mechanics.

Wave propagation across the fringe of ice floes separating the interior polar pack from the open ocean is a complex process. As ice approaches the ice edge from the far interior it encounters wave energy of gradually increasing intensity and gradually decreasing peak period, giving a steadily increasing degree of flexure to the vast ice sheets. Eventually the flexure causes the ice to break up into fragments, which themselves break again nearer the edge until a distribution of floe sizes is established with the smallest floes in the steepest wave field at the extreme ice edge. The floes thus created act as a shield for the interior pack, selectively damping out the shorter waves.

If the wind is blowing away from the pack, the floes diffuse to produce an open ice field (or else organize themselves into bands). So long as the floes do not collide, the wave attenuation process can best be described by a scattering model. As soon as the pack becomes closer (e.g. with an on-ice wind) floe collisions occur, generating high noise levels; a very compact pack behaves hydrodynamically either as a collection of very large floes or as a single entity. Since the floes can no longer surge in response to the waves, energy attenuation may be occurring more significantly in the form of viscous losses from the boundary layer under the ice.

Further into the ice, where very large floes exist, wave energy propagates as flexural-gravity waves, with losses occurring either as reflections from leads or from pressure ridges, or as creep hysteresis losses due to flexure of the ice sheet. New wave energy can be created within such a continuous cover by a sufficiently strong wind or other processes, but the energies involved are very small and can only be detected by sensitive instruments.

Finally, vast areas of shore-fast sea ice (Armstrong et al 1973) skirt the boundaries and fill the harbors and inlets of the landmasses of the Arctic Ocean and the Antarctic continent. In regions sheltered from ocean waves and swell, these ice sheets may grow over several years to great thickness, while in most cases they will be broken up into ice floes by storm seas in

the spring or will decay during the summer melt. Waves enter the ice sheet as flexural-gravity waves, causing the ice to flex rhythmically with their passing. If this flexing induces stresses that are greater than the ice can sustain, then fracture occurs, allowing part of the ice sheet to strip away. The remaining ice will then be subjected to analogous stresses and will fracture similarly. The systematic destruction of an ice sheet by this means is a rapid process which is a common occurrence, particularly where ice sheets abut open water.

In this review the following values are used for certain physical quantities: Young's modulus for sea ice,  $E = 6 \text{ GPa}$ ; Poisson's ratio for sea ice,  $\mu = 0.3$ ; density of sea water,  $\rho = 1025.0 \text{ kg m}^{-3}$ ; and density of sea ice,  $\rho' = 922.5 \text{ kg m}^{-3}$ .

## 2. OCEAN WAVES IN THE MARGINAL ICE ZONE

Both wave-induced break up and long-range swell propagation into the polar ice cover depend on the way in which waves propagate from the open ocean through the outermost fringe of broken floes—the marginal ice zone (MIZ). The problems here are to understand how waves propagate in such an ice field, how they are scattered and attenuated, how the waves cause the floe size distribution itself to become modified by flexural break up of individual ice floes, how waves contribute to ice margin dynamics, and how attenuation is balanced by wave generation when the ice field is diffuse. Included in this theme is the problem of ambient noise generation in the MIZ due to wave-induced floe collisions, and the relationship between the noise spectrum, sea state, and ice conditions.

### 2.1 *Solitary Ice Floes*

We begin with a discussion of the behavior of the ice floes themselves in waves as it is strictly this, together with floe-floe interactions, that determines the nature of all wave-ice phenomena in the MIZ. When acted upon by a train of ocean waves a solitary ice floe has six rigid-body degrees-of-freedom in which it can respond, i.e. heave, surge, sway, pitch, roll and yaw, together with its flexural response. Ice floes respond like any other floating, shallow draft body, although because of the mechanical properties of the sea ice a floe probably flexes to a greater extent than, say, a ship. For any such body undergoing oscillatory motion under the influence of surface waves, the magnitude of the motion depends on the height and frequency of the incoming waves. For wave height-to-length ratios of no greater than  $1/30$  it has been observed in full-scale trials and model experiments that the displacement of the body from its equilibrium position is linearly proportional to wave height (Lee 1976).

It is known that when a floating body undergoes motion in a fluid, there exists a hydrodynamic effect on the body that contributes additional mass or inertia. This so-called added mass is frequency dependent. For bodies of large length/thickness ratio—like an ice floe—added mass is small, but it becomes greater as the ratio decreases (Rumer et al 1979). In performing its “motions” the floating body generates a chain of progressive outgoing waves in the free surface, and a certain fraction of the energy supplied to the body to sustain its motion is utilized in creating these outgoing waves. Within a linear, rigid-body theory the energy loss due to the generation of surface waves is directly associated with the damping force of the body. Although this is only approximately true for an inelastic ice floe that bends significantly to the wave’s profile, it is likely to be the most significant damping term.

**OBSERVATIONS** During the 1970s and 1980s the Scott Polar Research Institute of the University of Cambridge, England, undertook a series of experiments in the waters off East Greenland and in the Bering Sea to study the motion and flexure of single ice floes in waves. At the same time some theoretical work was undertaken to describe their observations. The overall aim of the experimental program and the modeling was to understand the phenomenon of wave propagation through a MIZ. This was to be done by intensive experiments to characterize thoroughly the response of single ice floes to ocean waves and by transects where many ice floes in a line back from the ice edge were investigated in a less intensive way. Results from these experiments are found, for example, in Wadhams (1975, 1978), Squire & Moore (1980), and Wadhams et al (1986, 1988) in connection with the MIZ as a whole. Goodman et al (1980), Squire & Martin (1980), and Squire (1983) present a few results for single ice floe experiments; the remaining data have proved to be very difficult to interpret. Summarizing these data, we find:

1. Ice floes respond perfectly in heave at long wave periods, but their response is negligible for very short waves. Between these two limits the floe can resonate with an “intensity” that depends on the length/thickness ratio of the floe.
2. For short and very long waves, ice floes roll negligibly. At an intermediate wavelength, the roll response attains a maximum.
3. The strain transfer function for a bending ice floe of typical MIZ dimensions is such that it tends to amplify the shorter period components of the ocean wave spectrum. Thus the strain energy spectrum measured at the surface of an ice floe will usually have greater bandwidth than the open ocean spectrum that generates it.
4. Ocean waves may easily generate sufficient strain in an ice floe to cause

it to fracture when the length of the floe is a significant fraction of the wavelength or longer.

Further discussion on observations relating to the motion of individual ice floes in the MIZ may be found in Section 2.2, where we discuss floe-floe interaction. We now describe two theoretical models which were originally developed to study wave propagation through fields of ice floes, rather than to characterize fully the motions and flexure of solitary ice floes.

The boundary value problem to be solved is as follows. A solitary ice floe occupying  $0 \leq x \leq l$ ,  $z = 0$  floats on the equilibrium surface of the ocean, which is assumed to be infinitely deep (Figure 1). We require two-dimensional motion and flexure of the raft when acted upon by a train of small-amplitude surface gravity waves propagating in the direction of the positive  $x$ -axis. The floe is assumed to be in contact with the water at all points for all time. In terms of the velocity potential  $\Phi$  the system to be solved is

$$\nabla^2 \Phi = 0, \quad 0 < z < \infty, \tag{1}$$

$$\frac{\partial \Phi}{\partial z} = 0, \quad z \rightarrow \infty, \tag{2}$$

$$\frac{\partial \Phi}{\partial z} = -\frac{\partial w}{\partial t}, \quad z = 0, \tag{3}$$

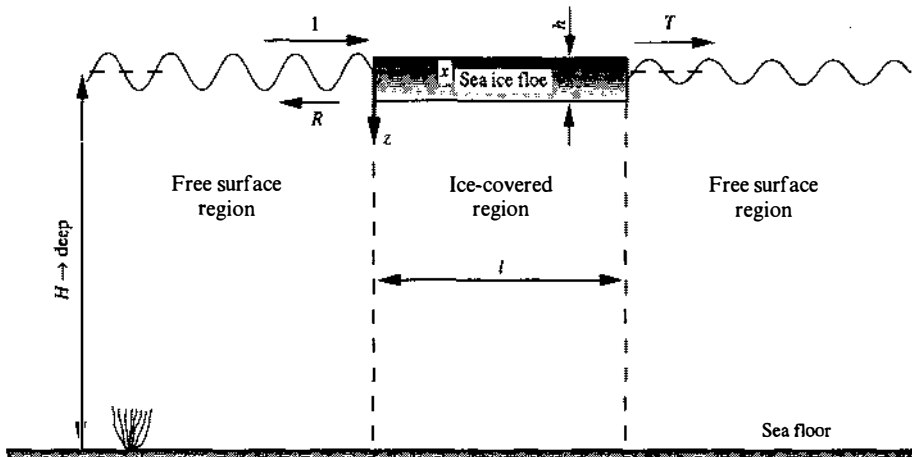


Figure 1 The two-dimensional geometry. A long-crested monochromatic wave incident normally on an ice floe of infinite width.

$$-\rho \left( g \frac{\partial \Phi}{\partial z} - \frac{\partial^2 \Phi}{\partial t^2} \right) = -\frac{\partial p}{\partial t}, \quad z = 0, \quad (4)$$

where  $w$  is the surface displacement of the water,  $p$  is the pressure on the water surface,  $\rho$  is the density of the water, and  $g$  is the acceleration due to gravity. We also require appropriate conditions to be met as  $x \rightarrow \pm \infty$  and at  $t = 0$ . Except over the raft ( $0 < x < l$ ), we assume  $p$  to be constant. Over the floe it is common to use the Bernoulli-Euler elastic thin plate model for the deflection, neglecting gravity effects, as follows:

$$\frac{\partial^2 w}{\partial t^2} + \gamma^2 \frac{\partial^4 w}{\partial x^4} = \frac{p}{\rho' h}, \quad z = 0, \quad 0 < x < l, \quad (5)$$

where  $\rho'$  is the ice density,  $h$  is its thickness, and  $\gamma^2 = Eh^2/12\rho'(1-\mu^2)$  where  $E$  is the effective Young's modulus and  $\mu$  is Poisson's ratio. Thus the boundary conditions beneath the floe and open sea are respectively

$$-\rho \left( g \frac{\partial \Phi}{\partial z} - \frac{\partial^2 \Phi}{\partial t^2} \right) = \rho' h \left( \frac{\partial^3 \Phi}{\partial t^2 \partial z} + \mu^2 \frac{\partial^5 \Phi}{\partial x^4 \partial z} \right), \quad z = 0, \quad 0 < x < l, \quad (6)$$

$$-\rho \left( g \frac{\partial \Phi}{\partial z} - \frac{\partial^2 \Phi}{\partial t^2} \right) = 0, \quad z = 0, \quad -\infty < x < 0, \quad l < x < \infty. \quad (7)$$

Additional transition conditions, namely, that the bending moment and shear must vanish at the ends of the raft, make the problem well posed:

$$\frac{\partial^2 w}{\partial x^2} = \frac{\partial^3 w}{\partial x^3} = 0, \quad \text{at } x = 0, \quad \text{and } x = l. \quad (8)$$

**THE WADHAMS MODEL** This model was developed in the early 1970s. As above it treats each ice floe as a floating elastic raft; the equations are solved approximately for the velocity potentials at the leading and trailing edges of the raft by matching. Within the raft itself the energy propagates as a flexural-gravity wave with an altered dispersion relation. The ice floe therefore scatters incoming ocean wave energy due to an impedance mismatch between the mode of propagation beneath the raft as compared to that under an open water surface. The treatment yields an energy reflection coefficient from which, for example, an attenuation rate for a collection of such rafts can be derived. Floe diameter appears to be a more critical parameter than ice thickness.

In the Wadhams model a complete solution for the matching of velocity potentials across the ice floe edge was not achieved. This has since been accomplished for a semi-infinite floe by Fox & Squire (1990, 1991b, 1994),

and for an ice floe of finite length using a Green's function approach by Meylan & Squire (1993a,b,c, 1994a).

The Wadhams model is described in full in Wadhams (1973a, 1986).

**THE MEYLAN & SQUIRE MODEL** The Meylan & Squire model begins by rewriting system (1–8) in nondimensionalized form using an integral equation for the under-ice boundary condition. Assuming that  $\Phi(x, z, t)$  can be separated into a time-independent part  $\phi(x, z)$  and a time-dependent (periodic) part:

$$\nabla^2 \phi = 0, \quad 0 < z < \infty, \tag{9}$$

$$\frac{\partial \phi}{\partial z} = 0, \quad z \rightarrow \infty, \tag{10}$$

$$\frac{\partial \phi}{\partial z} + \alpha \phi = 0, \quad z = 0, \quad -\infty < x < 0, \quad 1 < x < \infty, \tag{11}$$

$$\phi_z(x, 0) = -\frac{\alpha}{\beta} \int_0^1 g(\xi, x) \phi(\xi, 0) d\xi \quad z = 0, \quad 0 < x < 1, \tag{12}$$

$$\lim_{x \rightarrow \infty} \phi = T e^{-i\alpha x - \alpha z} \quad \text{and} \quad \lim_{x \rightarrow -\infty} \phi = e^{-i\alpha x - \alpha z} + R e^{i\alpha x - \alpha z}, \tag{13}$$

where  $R$  and  $T$  are the potential reflection and transmission coefficients, respectively. In this system the quantity  $\alpha$  is a nondimensionalized version of the open water wave number  $k = \omega^2/g$ , where  $\omega = 2\pi/\text{period}$  is the radian frequency. The quantity  $\beta = L/16\rho g l^4$ , where  $L = E h^3/12(1 - \mu^2)$  is the flexural rigidity of the ice. The kernel  $g(\xi, x)$  is a Green's function satisfying

$$\frac{d^4 g(\xi, x)}{d\xi^4} + \left( \frac{1 - \alpha \rho' h^3 \rho l}{\beta} \right) g(\xi, x) = \delta(\xi - x), \tag{14}$$

together with boundary conditions

$$g_{\xi\xi}(0, x) = g_{\xi\xi}(1, x) = g_{\xi\xi\xi}(0, x) = g_{\xi\xi\xi}(1, x) = 0. \tag{15}$$

Equations (9–13) are solved by using Green's theorem in the plane, together with the Green's function  $f$  for the ice-free, open water half space, e.g.

$$G(\xi, \eta; x, z) = \frac{1}{4\pi} \ln [(\xi - x)^2 + (\eta - z)^2] - \frac{1}{4\pi} \ln [(\xi - x)^2 + (\eta + z)^2] - \frac{1}{2\pi} \int_{\alpha}^{\infty} \frac{1}{|\omega| - \alpha} e^{-|\omega'(\eta + z)|} e^{i\omega(\xi - x)} d\omega, \tag{16}$$

to obtain a Fredholm integral equation of the second kind in  $\phi$  at the surface, with kernel

$$K(\zeta, x) = \frac{i\alpha}{2} [e^{i\alpha x} I(\zeta, -x) + e^{-i\alpha x} I(\zeta, x)] - \frac{\alpha}{2\pi} \int_{-\infty}^{\infty} \frac{e^{-i\omega x}}{\omega - \alpha} I(\zeta, \omega) d\omega, \quad (17)$$

where

$$I(\zeta, \omega) = e^{i\omega z} - 1/\beta \int_0^{\sigma_1} e^{i\omega \zeta} g(\zeta, \zeta) d\zeta.$$

The solution proceeds straightforwardly (Meylan & Squire 1993a,b) using the Nystrom method with Simpson quadrature. An energy flux condition  $|R|^2 + |T|^2 = 1$  serves as a check that the model has converged to the correct solution. The finite depth version of system (9–13) is solved similarly by Meylan & Squire (1994a).

In Figure 2 the magnitude  $|R|$  is plotted against floe diameter for several ice thicknesses. Each curve has the same basic structure, comprising a series of concave down segments that drop to  $|R| = 0$  at their ends, so that  $|T| = 1$  there. Thicker ice clearly leads to higher maxima in  $|R|$  but, since the wavelength beneath the ice increases with thickness, the number of

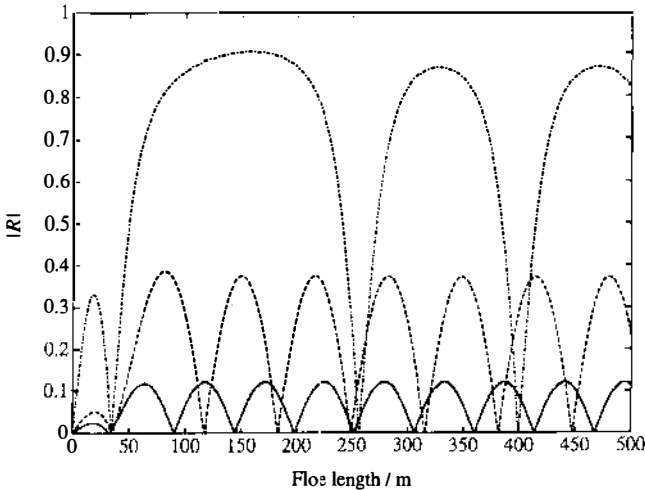


Figure 2 Reflection coefficient versus floe diameter for  $h = 0.5$  m (solid curve), 1 m (dashed curve), and 5 m (chained curve). Resonances at which  $|R| = 0$ , i.e. perfect transmission occurs, are clear. Wavelength is 100 m. After Meylan & Squire (1993a).

zeros for a specific floe diameter  $l$  varies inversely with floe thickness. The separation of the zeros tends to half the wavelength in the ice as  $l$  increases.

The surface strain induced in an ice floe of length  $l$  and thickness  $h$  is computed from

$$\epsilon = \frac{h}{2} \frac{\partial^2 w}{\partial x^2} = - \frac{h}{2i\sqrt{\alpha}} \frac{\partial^3 \phi(x, 0)}{\partial x^2 \partial z} \tag{18}$$

(Meylan & Squire 1993a,b). Although strain magnitude vanishes at the ends of the floe, in general it is nonzero in between, reaching a maximum at one or more points (Figure 3a). Figure 3a represents the strain magnitude transfer function for the specific ice floe being modeled with the incident wave amplitude normalized to 1 m. As period increases the maximum strain curve rises rapidly to a sharp peak, after which it decreases monotonically because long waves bend the ice less than short waves of the same height. The peak occurs because at short periods the floe's curvature is reduced by a large  $|R|$  (Figure 3b), whereas at long periods reflection is small. The fine structure is due to the reflection coefficient zeros discussed above, which occur at about 6.5 s and 13.5 s (Figure 3b). Strain transfer functions are influenced markedly by the reflection/transmission characteristics of the ice floe, with strain maxima likely to be found near wave periods where  $|T| = 1$ .

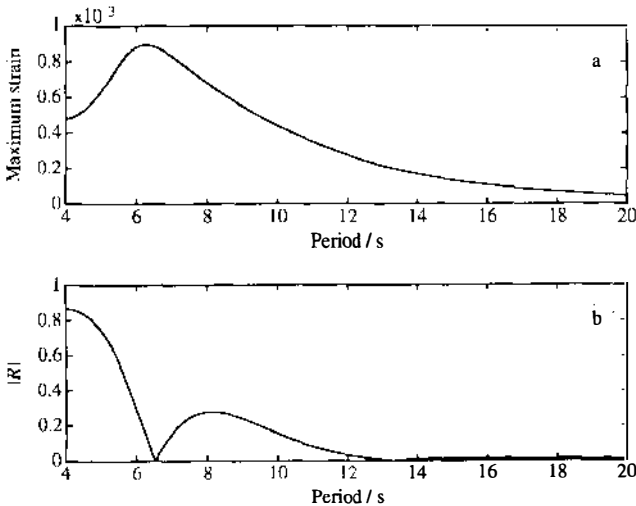


Figure 3 (a) The maximum surface strain magnitude experienced by the floe and (b) the magnitude of the reflection coefficient, both plotted against wave period for a  $100 \times 1$  m ice floe. After Meylan & Squire (1993a).

Although an advance on the Wadhams (1973a, 1986) model, the Meylan & Squire (1993a,b) model remains two-dimensional. This is its major limitation: An ice floe responding to an incoming wave field will scatter energy in all directions.

**OTHER MODELS** The model of Squire (1981, 1982) specifies a two-dimensional solitary ice floe of arbitrary cross-section, and its equations are solved numerically for the rigid body motions using discretized source distributions along the floe's underside (Frank 1967). The pressure field is then used to bend the ice via a finite element code. The method works well but is computationally unwieldy for application to many floes of different shapes and sizes.

**ADJACENT FLOES** An extension of the Meylan & Squire (1993a,b) model to a pair of separated elastic rafts (Meylan & Squire 1994a) allows the effect of a floe on an adjacent partner to be determined. It is found that the two floes must be very close for the first to affect significantly the second so that, unless the MIZ is very compact, results from two single floe models applied serially may be superimposed.

## 2.2 *Floe-Floe Interaction*

When floes respond to wave action in the marginal ice zone they tend to collide, since adjacent floes are moving out of phase with one another. The impulse associated with the collision results in momentum transfer and a concomitant loss of kinetic energy for inelastic events. Alternatively, two floes may be dragged past each other in shear. Then, unless the contacting areas are perfectly smooth, momentum is again transferred and kinetic energy is dissipated. Real ice floes also possess rotational as well as translational motion, so a real interaction event will comprise a combination of shearing and collision properties. Publications concerning interactions between adjacent ice floes, both reporting data and model development, may be grouped into the following categories:

1. The driving force leading to relative motion within the ice field.
2. The nature of individual interaction events.
3. The rate at which interaction events occur.
4. The consequences of individual floe pair interactions on the ice field.

**OBSERVATIONS** Accelerometer and tiltmeter packages have been extensively used to measure some or all of the six possible rigid-body motions that an ice floe may experience, but these instruments (especially horizontal accelerometers) also reveal the change in motion of a floe that results from an interaction with a neighbor.

The most comprehensive investigations of floe pair interactions to date

are those of Martin & Becker (1987, 1988) who use accelerometer data obtained from the Greenland and Bering Seas to address all four categories listed above. Vertical acceleration measurements were used to determine the mean-square wave amplitude as a function of time. Collision events led to very clear signatures in horizontal acceleration data, which were classified either as major, but infrequent, events—believed to be associated with the large-scale deformation of the ice field as they were uncorrelated with wave amplitude—or as events of much smaller magnitude but more frequent occurrence, which were highly correlated with wave amplitude. Up to about two events per minute occurred (see Figure 4). Each event was described in terms of the root-mean-square (RMS) collision velocity ( $\sim 1 \text{ mm s}^{-1}$ ) and the floe displacement associated with each collision ( $\sim 10 \text{ mm}$ ). Martin & Becker's principal conclusion is that the vast majority of floe collision events in the MIZ are driven by ocean swell. They report that collision-induced stresses are insufficient to induce ridge building events, and that collision-induced displacements do not contribute significantly to the deformation of the ice field as a whole.

McKenna & Crocker (1992) present accelerometer and tiltmeter data obtained at the Labrador Sea ice margin on considerably smaller floes than those of Martin & Becker. Their collision rates (up to a few per minute) were not well-correlated with wave amplitude, but did appear to be correlated with increasing wind speed and decreasing air temperature.

Rottier (1992) determined interaction event rates for the Barents and Greenland Seas in ice conditions similar to those of Martin & Becker. Their event signatures again showed up very clearly in horizontal acceleration time series, with the event rates taking values of up to a few per minute. Clusters of events occurred at times when the local wave amplitude—determined from the floe's vertical acceleration—was greatest (see Figure 5). Measured event rates did not correlate well with swell amplitude directly when a number of distinct experiments were combined, but did correlate with the ratio of RMS wave amplitude to the amount of open water between the floes. Observations suggested that brash (fragmented) ice between floes acted as an intermediary in the transfer of momentum from one floe to the next.

The MIZ is not invariably a wavy environment and driving forces unrelated to ocean swell must be considered as candidates for producing floe-floe interactions. As a result of their different dimensions and roughnesses, individual floes have varying responses to applied wind and current stresses. Guest & Davidson (1991) discuss the various atmospheric drag coefficients associated with ice of different types, and Dugan et al (1992) show that surface motions in pack ice may be driven by local pressure fluctuations in the atmospheric boundary layer at frequencies above about

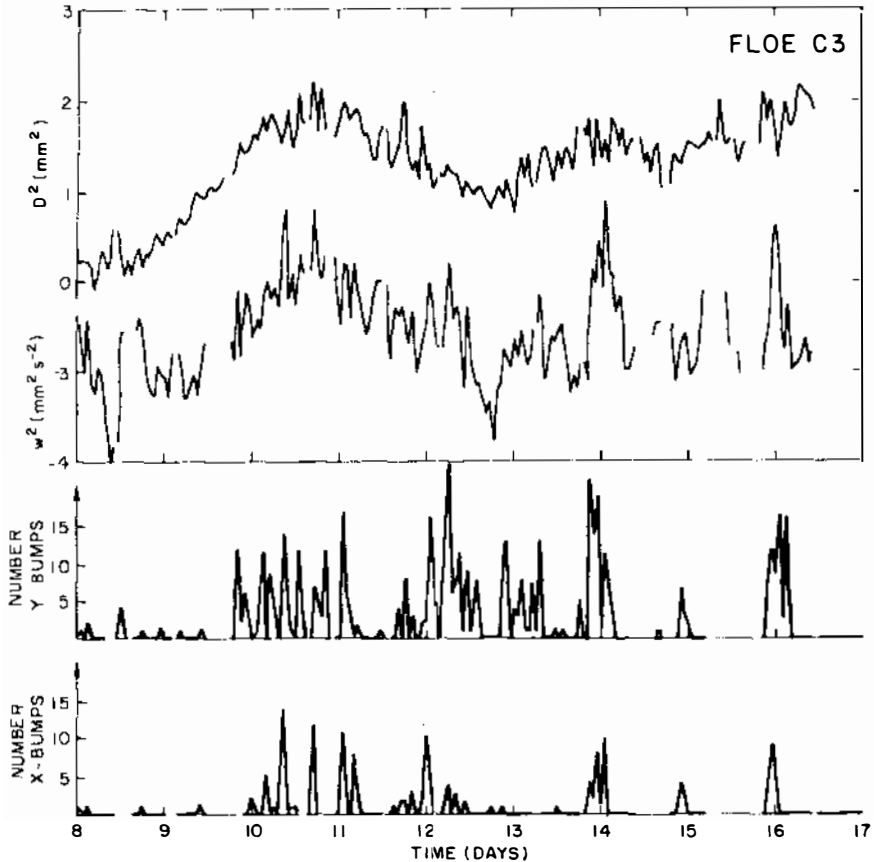


*Figure 4* An example of the strong correlation between the rate at which floe collisions occur and the amplitude of the incident ocean wave field. The upper trace, labeled  $D^2$ , is the logarithm of the mean-square wave height in  $\text{mm}^2$ , the trace labeled  $w^2$  is the log of the mean-square horizontal velocity in  $\text{mm}^2 \text{s}^{-2}$ . The remaining two traces show the number of floe collisions recorded during nine-minute intervals throughout the period of measurement. The two channels correspond to the two horizontal accelerometers used in the instrumentation package. Clearly, more collisions occur at times when the mean square wave amplitude is greatest, and for  $\log(D^2) \lesssim 1$ , events rarely occur. After Martin & Becker (1987).

0.05 Hz. Concomitant horizontal motions must result. Although not strictly based on MIZ data, Martin & Drucker (1991) identify three distinct types of interaction event: the shearing process, which leads to “stick-slip” and results in a saw-tooth acceleration time series; near-sinusoidal,  $\sim 1$  Hz, horizontal accelerations caused by cycles of crushing and clearing of debris from floe edges and associated with ridge building events; and the collision event, which occurred at times of ice divergence.

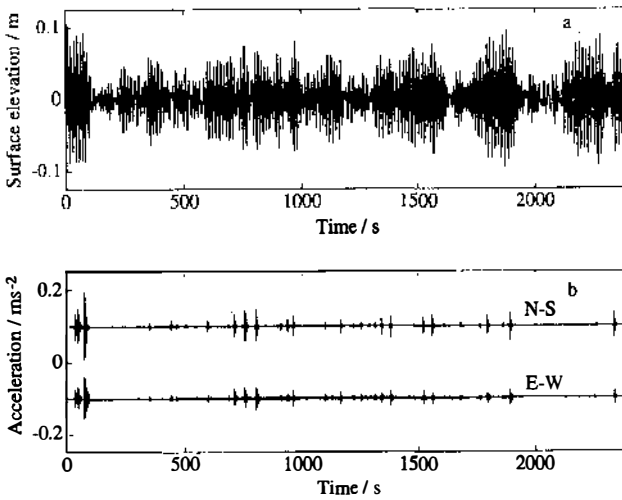


*Figure 5* Example of time series obtained from an accelerometer package deployed on an ice floe. (a) Time series of surface elevation in meters obtained by numerically integrating (twice) the vertical acceleration. (b) Horizontal accelerations resolved into north-south and east-west components and offset by plus and minus  $0.1 \text{ m s}^{-2}$  respectively for clarity. The large amplitude “spikes” in the horizontal acceleration are the result of collisions between the instrumented floe and its neighbors. (The normal horizontal accelerations associated with the motion of the floe are not discernible at this scale.) Collisions are dependent on the amplitude of the incident wave field in two ways: The magnitude of the signal associated with each event is generally greater at times when the amplitude of the wave field is greater; and events are grouped, more occurring at times when the vertical amplitude of the floe’s motion is greatest. After Rottier (1992).

**MODELING** Small-scale models are used for specific ice floes under specific conditions. The large-scale behavior of an ice field is modeled by making a number of assumptions about the way individual floes interact.

A wave-driven collision or shearing event between two floes is complicated to model. The problem is simple to pose in terms of the fluid’s velocity potential, but it is difficult to solve without recourse to several assumptions whose significance is hard to assess. Additionally, a knowledge of their mechanical interaction is needed for times when the ice floes are in contact.

McKenna & Crocker (1990) modeled the motion of ice cakes in the presence of a deep water, sinusoidal wave by assuming that the floes behave like small particles of fluid. Each floe center moves in a circular path, and if two are sufficiently close they may collide inelastically at some point during the wave cycle to destroy a small quantity of ice at each floe’s edge. McKenna & Crocker conclude that collisions are important for the

reduction in floe diameter as a function of time but cannot account for the observed decrease in wave energy as swell penetrates an ice field.

Following Rumer et al (1979), Shen & Ackley (1991) employ a floe sliding model of (surface wave)/(ice floe) interaction, including each floe's drift superposed on a sinusoidal oscillation. For two initially close floes, they demonstrate that collision events begin after a few waves have passed and recur during some subsequent wave periods. Collision contact forces are obtained with a spring-dashpot model. The exact frequency of events depends on wave amplitude, as well as the choice of restitution coefficient. From their model they also obtain an expression for the time the floes are in contact as a result of the collision. This is an important parameter as it may allow floes to coagulate to form larger composite floes. Shen & Ackley also demonstrate that floes are bunched into groups due to the incident wave, a phenomenon that can readily be observed in the MIZ.

Rottier (1992) also modeled relative floe motion to obtain a prediction of interaction event rates for floes of known dimensions, allowing for the randomly varying nature of real surface waves. Predicted rates were compared with measurements, and reasonable—though not conclusive—agreement was found.

On a larger scale, several models have been conceived to investigate MIZ rheology, which incorporate consequences of floe collisions (e.g. Bratchie 1984, Shen et al 1987, Lu et al 1989). In each case, floe collisions result from the large-scale deformation of the ice field; the additional effect of wave-induced collisions has not yet been included. During each collision, some kinetic energy is lost. The coefficient of restitution  $e$ , whose value lies between 0 and 1, defines the amount of the precollision energy dissipated; no measurement of its value for colliding ice floes is available at this time—the attempt by Rottier & Squire (1993) to determine  $e$  has produced equivocal results. Shen et al conclude that collisional stresses are small when compared to typical air stresses found in the MIZ.

Finally, Gao (1992) proposes a simple, perfect surge model, which was tested against observational evidence from the Labrador Ice Margin Experiment (LIMEX). Aerial photographs were analyzed to yield statistical distributions of spacings between centers of floes and edges. Gao showed persuasively that log-normal distributions provide the best fit for both. He then re-expressed the collision probabilities for two floes in terms of these distributions to yield estimates of collision rates, which he compared with observations made by accelerometers on the floes themselves. These differed by an order of magnitude. Gao's results, while not supportive of his theory, are important: They are a genuine and careful experimental test indicating that an important physical process has been omitted.

### 2.3 Wave Attenuation

The effect of pack ice in calming an incoming sea is well known. This must have been known for centuries to Inuits and to sealers and whalers working in ice-infested waters, though little has been written about the topic. It is only relatively recently that a concerted effort has been made to understand the phenomenon both by experiment and by the development of theoretical models.

**OBSERVATIONS** Extensive field observations of wave decay in MIZ regions have been conducted over the past two decades; some of the more recent measurements are described by Squire & Moore (1980) and Wadhams et al (1986, 1988). Techniques that have been employed include shipborne wave recorders (Robin 1963), upward sonar from a hovering submarine (Wadhams 1972, 1978), and airborne laser profilometry (Wadhams 1975), but most recent measurements have used a directional wave buoy in open water and diffuse ice, or a combination of accelerometers, strain gauges, and tiltmeters on ice floes performing an equivalent function to a directional wave buoy. The main conclusions from the observations are as follows:

1. The attenuation of waves with distance into the pack assumes a negative exponential form, with an attenuation coefficient that decreases with increasing wave period over most of the spectral range. In heavy compact ice (e.g. East Greenland) the energy attenuation coefficient typically varies from  $2 \times 10^{-4} \text{ m}^{-1}$  for the longest swell to  $8 \times 10^{-4} \text{ m}^{-1}$  for 8–9 s waves, corresponding to *e*-folding distances of 5–1.2 km.
2. There is some evidence of a “rollover” at the shortest periods (less than 6–8 s), where the decay rate may actually start to diminish as the wave period shortens.
3. The directional spectrum increases in spread inside the ice field until it is essentially isotropic within a few kilometers of the edge.
4. Some wave energy is reflected from the outer edge of the ice field (but only a few percent), even when the edge is compact.

**SCATTERING** A simple scattering model to explain some of these findings was developed by Wadhams (1973a, 1986). It assumes that floes of diameter  $l_j$  in the direction of the wave vector occupy a fraction  $p_j$  of the sea surface, and each has an energy reflection coefficient  $R_j$  computed from the solitary floe equations. The energy decay rate is then of the form

$$\frac{\partial E}{\partial x} = -2\alpha_x E,$$

where

$$\alpha_x = \frac{1}{2} \sum_j \frac{p_j R_j}{l_j} + o(R_j^2), \quad (19)$$

where summation is over the distribution of floe sizes present. The model matches experimental results at normal and long wave periods, but does not always predict the observed rollover at short periods. Other defects are that it does not predict increased directional spread as waves pass into the ice, and that the reflection coefficients it uses derive from an approximate solitary floe model. Despite these caveats the scattering model reproduces many of the observed features of MIZ wave attenuation.

An equivalent multiple scattering model based on the precise Meylan & Squire (1993a,b) model (Meylan & Squire 1994b, Squire & Meylan 1994) poses the equations in matrix form for incoherent addition of energies as

$$\begin{pmatrix} t_{j-1} \\ r_{j-1} \end{pmatrix} = \frac{1}{T_j} \begin{pmatrix} 1 & -vR_j \\ vR_j & T_j^2 - vR_j^2 \end{pmatrix} \begin{pmatrix} t_j \\ r_j \end{pmatrix}, \quad (20)$$

where  $R_j$  and  $T_j$  are the energy reflection and transmission coefficients of the  $j^{\text{th}}$  of  $n$  floes, and waves of energy  $t_j$  and  $r_j$  impinge on that floe from the left and right, respectively. The parameter  $v$  allows additional damping to be introduced between adjacent ice floes. Without loss of generality  $t_0 = 1$  and  $r_n = 0$ . A distribution of ice sizes of any type may be incorporated, as can changes in concentration  $c$  via a rescaling of penetration  $d$  to  $100d/c$ .

The normalized energy  $t_n$  computed for a Rayleigh distribution of ice floes of mean diameter 100 m and thickness 1 m decreases from 1 at low frequencies to 0 at high frequencies, with most of the change occurring in a sharp transition band when many floes are present (Meylan & Squire 1994b). Thus the model predicts that the ice should behave as a low-pass filter, in agreement with observations generally—though no evidence of the observed rollover is reported at the shortest periods. The original Wadhams (1973a) model can produce rollover to some extent but its onset does not always match the data well.

The scattering model gives a good fit to many of the wave measurements done in ice where floe size distributions were measured concurrently (Wadhams et al 1988). It is inadequate, however, in the following ways:

1. For real floe size distributions, high frequency rollover is not always evident.
2. The model takes no account of directional spread. It was suggested by Wadhams (1978) that the directional spread of an incident spectrum should become narrower within an ice field and more concentrated along a bearing normal to the ice edge. This is because at any distance

$x$  from the ice edge, wave components with an angle of incidence  $\theta$  will have traveled a distance  $x \sec \theta$  through ice and will therefore have suffered an attenuation which increases with  $\theta$ . These ideas were corroborated recently by Squire & Meylan (1994). In contrast, the field experiments of Wadhams et al (1986) indicate that the directional spectrum widens with penetration until it becomes isotropic. This was especially true at short periods: A 3.3 s component became isotropic within 1.2 km, 4.1 km, and 0.7 km of the ice edge in three separate experiments, while the swell component took up to 17.8 km to become isotropic and did narrow in the earliest stages. We conclude that the collimating effect competes with a lateral scattering effect, whereby energy lost from the forward-going wave vector is not only back-scattered but is also scattered with a directional spread, so that a floe in the far interior is bathed in scattered radiation from surrounding floes, with a weakened forward-going vector. A mathematical model of two-dimensional scattering from an ice floe, which can describe the magnitude of this spread, is still required.

3. When the model is used to predict wave reflection from the front of an ice field it usually predicts reflection coefficients in excess of the 2.6–12.7% energy reflection coefficients observed by Wadhams et al (1986).

The scattering model does not predict any change in dispersion on entry into the ice field, as it considers only the perturbations to the forward-going wave energy vector produced by individual floes. Support for this idea came from the Wadhams et al (1986) experiments, where no refraction was observed across the ice edge, but more recent observations from satellite synthetic aperture radar (SAR) images do suggest refraction and therefore a change in dispersion (Liu et al 1991b). It is an open question at present whether this refraction is due to the ice type being other than that of separate moderate floes, or whether the scattering model can be considered inadequate in this area too.

**VISCOUS MODELS** As an ice field becomes more compact the interactions between floes increase and it is often unrealistic to consider the ice field as being composed of individual floes. Instead, floes collide, or are held together by an on-ice wind or by freezing of brash, pancake, or frazil ice (Armstrong et al 1973). Such an ice field approaches the condition of being a single entity and it is tempting to ignore the detailed physics of the many kinds of energy-consuming, ice-water and ice-ice interaction processes that are occurring, and instead model the ice cover as a material with empirically determined properties, which covers the sea surface and attenuates waves.

The simplest such material is a collection of noninteracting mass points,

i.e. a load on the sea surface with no strength properties of any kind. The theory of wave propagation in this material was developed in the 1950s, and recent data suggest that it may be applicable to frazil and pancake ice types (see the next subsection).

An upper limit for energy losses in the boundary layer was found by Wadhams (1973a). He estimated dissipation under ice by assuming realistic skin-friction and form drag coefficients, and the existence of a quasi-static boundary layer. With a variety of assumptions about possible ice roughnesses, the wave amplitude decay coefficient due to viscous losses was always at least an order of magnitude less than that due to scattering. Wadhams concluded that viscous losses are insignificant to scattering losses.

Using a Lagrangian formulation, Weber (1987) introduced the idea of the ice cover as an asymptotically thin, highly viscous Newtonian fluid on a rotating ocean, and obtained reasonable agreement with observations. Liu & Mollo-Christensen (1988) describe an alternative model which proposes that attenuation is due to the viscous boundary layer under ice. It is assumed that in a highly compact ice cover, where ice floes are held together by wind stress or partial freezing of interstitial material, waves disperse as though propagating beneath a thin elastic sheet. An oscillating boundary layer develops under the ice, causing energy loss, which is parameterized by a phenomenological eddy viscosity  $\nu$  related to the actual flow conditions.

The model does predict the desired rollover at short wave periods, and its predictions can be made to agree with the field data of Wadhams et al (1988) and SAR data from LIMEX. The onset of rollover depends on the ice conditions, and especially on ice thickness (Liu et al 1991a). However, the tuning parameter—the turbulent eddy viscosity, which is used to measure the mixing level in the turbulent boundary layer—takes on a wide variety of values. [Liu et al (1992) found that the two LIMEX experiments required values of 290 and 12  $\text{cm}^2 \text{s}^{-1}$  respectively to provide a good fit, while to fit the data of Wadhams et al (1988), values from 4 to 1536  $\text{cm}^2 \text{s}^{-1}$  were required.] This is an undesirable feature of Liu et al's model; to overcome the problem, Liu et al (1992) propose—based on the interpretation of several field experiments—that  $\nu$  should be a linear fraction of  $(chH_s/\text{period})$ , where  $H_s$  is significant wave height. More development of these ideas is needed before they can be used for the prediction of decay rates.

In the model of Liu et al (1991a, 1992) all forms of energy loss are forced into the bin of viscous loss, thereby requiring a high (phenomenological) eddy viscosity to produce sufficient loss to match observations. Wadhams' viscosities, on the other hand, derive from physically-based roughness

arguments. Thus the apparent disagreement between conclusions is resolved.

**MASS-LOADING MODELS** This was the first class of models developed to describe wave-ice interaction, but at the time (1950–1953) no data existed to validate the theory. Ice is visualized as a continuum composed of noninteracting mass points which exerts a pressure upon the water surface but which has no coherence or rheological properties. The theory was developed by Peters (1950), Weitz & Keller (1950), Keller & Weitz (1953), and Shapiro & Simpson (1953), and is summarized by Wadhams (1986), who pointed out an error in the treatment by Shapiro & Simpson. [Unfortunately the error was inadvertently repeated in a paper by Wadhams & Holt (1991).] Originally the theory was envisaged as appropriate for all kinds of ice fields, but Wadhams & Holt (1991) make the case that it is appropriate only for describing wave propagation in frazil and pancake ice.

Following Wadhams (1986) the wave number  $\kappa$  for propagation in ice is given by

$$\kappa = \frac{\rho\omega^2}{\rho g - \rho'} = \frac{k}{\quad} \quad (21)$$

Thus a wave propagating into the ice from open water acquires a reduced wavelength  $\lambda = 2\pi/\kappa$ . This has the following implications:

1. Obliquely incident waves are refracted toward the normal.
2. Waves entering the ice acquire a greater amplitude and steepness.
3. A frequency limit is implied in (21), given by

$$\omega_c = \left( \frac{\rho g}{\rho' c h} \right)^{1/2}, \quad (22)$$

above which propagation is impossible.

Amplitude reflection and transmission coefficients  $R$  and  $T$  across the ice edge were derived by Keller & Weitz (1953), and the correct forms were given in the review by Wadhams (1986, p. 924), with equations (17) and (18) in Wadhams & Holt (1991) being incorrect. The correct forms are

$$(1 - |R|^2) = |T|^2 \frac{k^2}{\kappa^2}, \quad (23)$$

giving an energy transmission coefficient for normal transmission of

$$|T|^2 = \frac{4\kappa^3}{k(k+\kappa)^2}. \quad (24)$$

Wadhams & Holt showed that dispersion relation (21) could explain wave refraction in frazil and pancake ice observed on *Seasat* SAR in the Chukchi Sea, yielding realistic (although somewhat large) values for frazil slick thickness.

Although the mass-loading model does not yield any progressive wave decay, it does imply wave refraction at the ice edge and the total exclusion of the shortest waves from the ice field. Clearly, energy decay does take place in frazil slurries, and Martin & Kauffman (1981) observed an internal circulation within the slick in tank experiments, which would lead to viscous energy losses. Further research on this mechanism is needed.

The model has also recently been applied to an ice field with spatially varying concentration by Squire (1993c), who treats the open ocean as analogous to free space, and zones of different concentration as layers of different "refractive index"  $n_j$ , determined by the dispersion relation (21). If one denotes the surface density of the  $j^{\text{th}}$  zone as  $m_j = \rho'c_jh_j$ , where  $c_j$  and  $h_j$  are concentration and thickness, respectively, then

$$n_j = \frac{1}{(1 - m_j\omega^2/\rho g)}. \quad (25)$$

Squire (1993c) considers transmission and reflection on entry to the ice cover and at each change of surface density, assuming, in the manner of a WKB approximation, that reflected waves are damped before they reenter the  $(j-1)^{\text{th}}$  zone. Further dissipation is imposed using eddy viscosity damping. The model is then compared with two sets of observations: a band experiment done during the 1986 Winter Weddell Sea Project (WWSP) and an attenuation experiment done in the Bering Sea in 1979. In both cases Squire's model tends to predict attenuation coefficients that increase too rapidly with frequency because condition (21) guarantees that the wave number in ice is greater than that in open water, i.e.  $n_j > 1$ , with the result that the eddy viscosity parameterization increases rapidly with frequency.

## 2.4 Floe Breakup

Thus far we have considered waves entering an ice field with a specified distribution of floe diameters. In practice the MIZ is rarely, if ever, in equilibrium; the incident sea state is constantly changing while random ice motion is constantly bringing large floes within range of the ice edge, where they are broken up to alter the attenuation rate of the waves. There

is thus a tendency (never completed) towards an equilibrium state in which the floe size at any penetration does not exceed a critical value above which flexural failure would occur. It is important, therefore, to understand the failure criterion and flexural response of a floe that is bending in a wave field. The problem was first tackled by Goodman et al (1980) who, as well as developing a simple theory, reported an observed fracture strain of  $\sim 3 \times 10^{-5}$  for East Greenland sea ice, noting that fracture toughness arguments would suggest that a crack will propagate if the strain reaches  $4.3 \times 10^{-5}$ . Consistent with these results Squire & Martin (1980) deduce the fracture strain for Bering Sea ice to be  $4.4-8.5 \times 10^{-5}$ . Goodman et al's theory has subsequently been applied to the breakup of tabular icebergs (Wadhams et al 1983). The more sophisticated model of Squire (1981, 1982) could easily be used as an alternative to the approximate Goodman et al model.

Later in Section 3 we discuss the breakup of ice sheets; many of the conclusions there are relevant to the breakup of vast ice floes embedded within the MIZ (Squire 1993a).

Finally, we note that M. Lensu (personal communication, 1991) presented a paper entitled "The Evolution of Floe Distributions" to the December 1991 IAPSO Workshop on Wave-Ice-Interaction (Wadhams et al 1992). The formal model reported describes how a floe size distribution evolves with time, given a specified breakup rate. This would form an essential component of any MIZ equilibrium model.

## 2.5 *Wave Observations by SAR*

The ability of a synthetic aperture radar to provide valuable information on the type, condition, and motion of the ice cover is well demonstrated. SAR images of the ocean surface from the *Seasat* satellite have shown that refracting surface waves, wind signatures, oceanic fronts, and meso-scale eddies can be detected through their influence on the short wind waves responsible for microwave backscatter (Fu & Holt 1982). Similar surface signatures of swell, wind, fronts, meanders, and eddies have also been observed near the ice edge by SAR from satellites (*Seasat*, *SIR-B*) and by airborne radars (Carsey et al 1986, Wadhams & Holt 1991).

Although SAR imaging of ocean surface waves has been demonstrated by many, the relative importance of imaging mechanisms such as hydrodynamic modulation, tilt modulation, and velocity bunching is still not well understood (Alpers et al 1981, Hasselman et al 1985). Recently, extensive research has been conducted, as reported by Beal (1987), and by Shemdin (1988) from the Tower Ocean Wave And Radar Dependence Experiment (TOWARD). It is generally accepted that the dominant mechanism that allows a SAR to image waves in an ice field is velocity bunching

(Lyzenga et al 1985, Liu et al 1992)—a natural consequence of coherently sensing scatterer motions at the wave orbital velocity.

Using SAR imagery the spatial variability of the sea's dominant wavelength may be estimated by means of spectral analysis. Figure 6 shows a C-band SAR image of sea ice taken on March 23 off Newfoundland during LIMEX'87. The image shows the swell penetrating into the MIZ and a periodic displacement of the ice-water boundary, apparently due to velocity bunching effects associated with the orbital motions of the waves. Note the clearly discriminated shear line, which indicates the extent of detectable swell penetration and the penetration at which ice rafting and compaction are significant. On the basis of the wave spectrum found from the SAR data, together with concurrent wave frequency spectra computed from ocean buoy data and time series from an accelerometer package placed on the ice, Liu et al (1991a) were able to estimate the dispersion relation. An altered wave dispersion within the ice cover suggests that refraction should occur at the ice edge (Squire 1984c, Liu & Mollo-Christensen 1988, Fox & Squire 1994) and this was observed in the SAR imagery during the LIMEX'87 experiment (Liu et al 1991b).

Wave attenuation in the MIZ during LIMEX has been studied by Liu

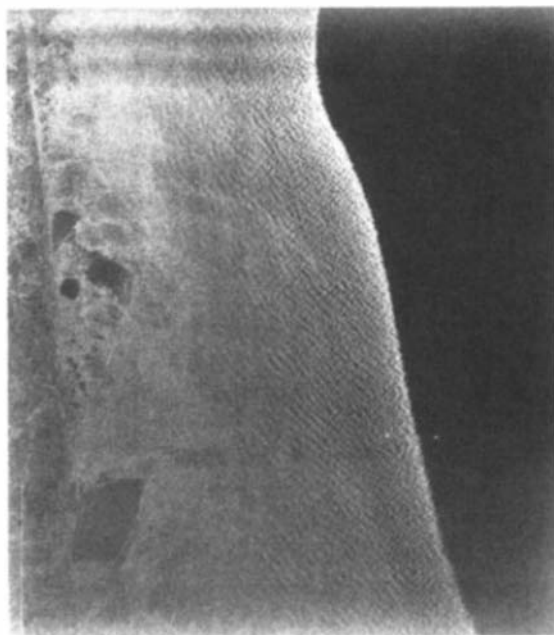


*Figure 6* C-Band SAR image of sea ice and swell impinging on the ice margin. The image was taken off Newfoundland during LIMEX'87. After Liu et al (1991a).

et al (1992). As an example, representative SAR spectra with 1-dB contour steps at (a) 0, (b) 6, (c) 12, and (d) 18 km along the wave propagation direction from line 2, pass 5 on 28 March 1989 are shown in Figure 7. The ambiguous spectral lobe has been crossed out. By extracting many SAR subscenes in the wave propagation direction and estimating the decreasing contrast for each wave number band, the wave attenuation coefficient is obtained from SAR data as shown in Figure 8 for LIMEX'87 and LIMEX'89. The SAR data show the same rollover at high wave numbers

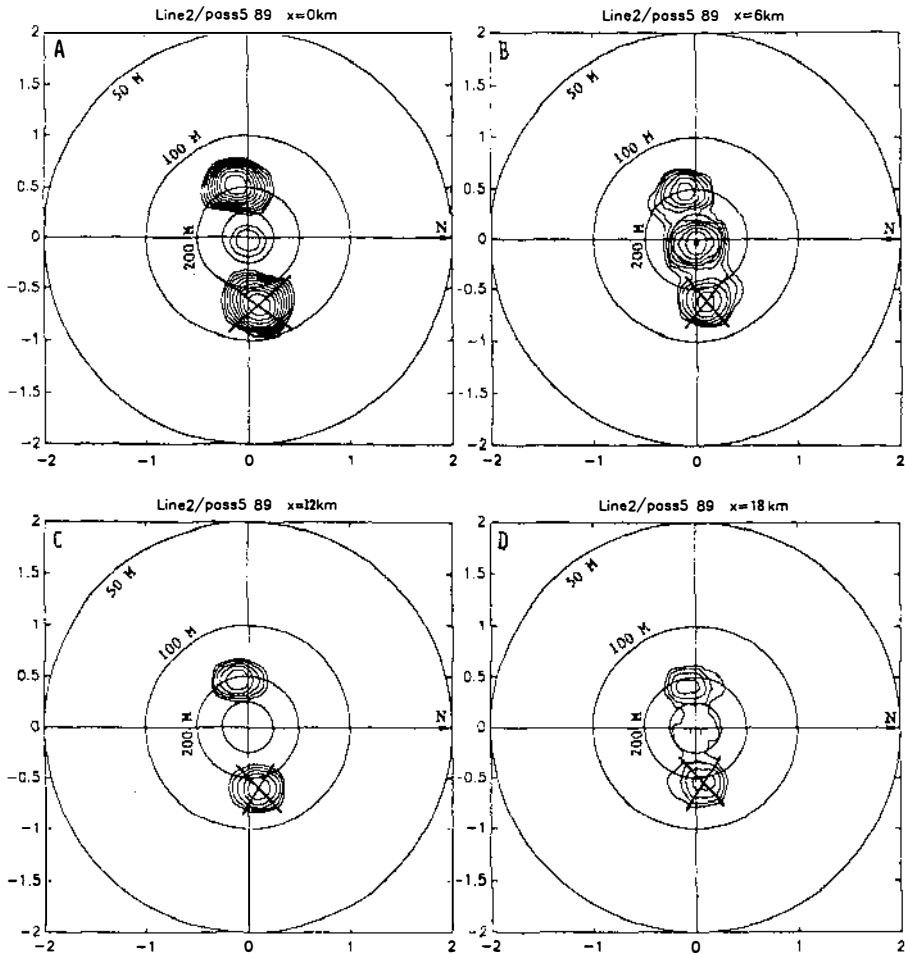


Figure 7 Representative SAR spectra with 1-dB contour steps at (a) 0, (b) 6, (c) 12, and (d) 18 km along the wave propagation direction from LIMEX'89. After Liu et al (1992).

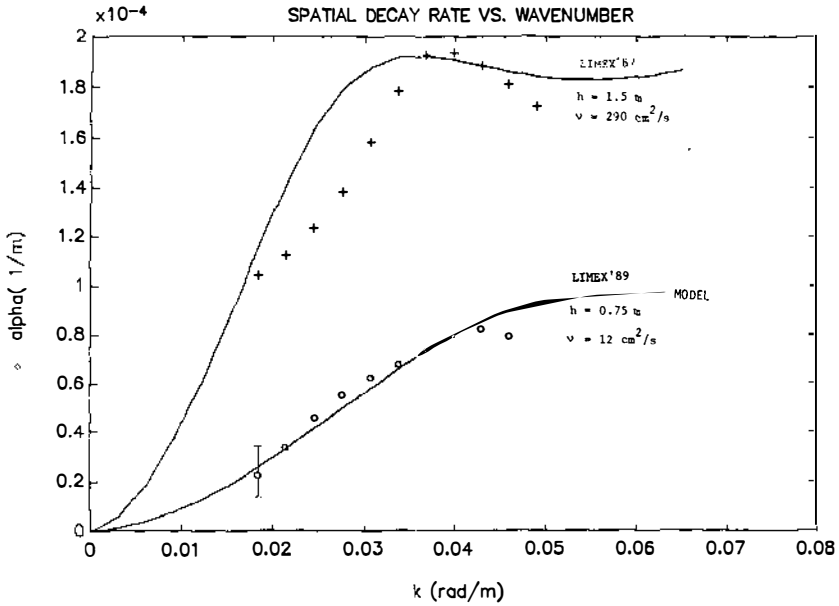


Figure 8 Model-data comparisons for wave attenuation coefficient as a function of wave number for LIMEX. After Liu et al (1992).

seen in the ice-motion sensor data of Wadhams et al (1988) and referred to earlier. The smooth curves drawn on the data result from the viscous attenuation model of Liu & Mollo-Christensen (1988).

## 2.6 Wave Radiation Stress and Ocean-Ice Interaction

The indication in SAR imagery that refraction away from the normal can occur at an ice edge (Liu et al 1991b) suggests that for some highly concentrated MIZs, which form a continuum rather than a matrix of discrete scatterers, the dispersion relation within the ice is different from that in the open sea. Because the angle of refraction exceeds the angle of incidence, the mass-loading boundary condition (21) can immediately be dismissed. The inclusion of rigidity has the desired effect and a suitable boundary condition is the same Bernoulli-Euler condition (5) seen earlier but applied over the entire marginal ice zone. Such dispersion also suggests the existence of a critical incidence angle beyond which "total external reflection" occurs. Liu et al (1991b) report that the dominant swell disappeared locally in the SAR imagery where the ice edge had large curvature, and conclude that the local critical angle had been exceeded by the incoming swell.

Reflection at the ice edge, and especially total reflection, implies that

the ice edge must be subject to a mean horizontal force due to radiation stress:

$$F = \frac{1}{4} \rho g (1 + R^2 - T^2) (1 + 2kH/\sinh 2kH) \quad (26)$$

(Longuet-Higgins 1977) for unit incident amplitude, where  $H$  is the water depth. If wave propagation in a zone within the ice medium is such that the principal wave is gradually attenuated away, Squire & Fox (1991) assume that all of the momentum is absorbed by the zone. They then investigate the force density spectrum for typical ice covers subjected to an open water Pierson-Moskowitz spectral density (Phillips 1977). The magnitude of the wave-induced forces are found to be of the same order or larger than wind and current forces.

Squire (1989) considers what happens when all the incoming momentum is reversed, i.e. the critical angle is exceeded and waves are totally reflected at the boundary. Under these circumstances, the normal and shear forces per unit length are  $S_{xx} = S \cos^2 \theta$  and  $S_{xz} = (\frac{1}{2})S \sin \theta \cos \theta$ , respectively, where  $\theta$  is the angle of incidence and  $S$  is the total spectral energy density. Squire applies these results to the analysis of WWSP pitch-roll buoy data taken on either side of a consolidated band of pancake ice lying just outside the main MIZ. Using the maximum entropy analysis of Lygre & Krogstad (1986) to estimate the directional distribution, it is shown that the long period swell was unimodal whereas the shorter wind sea was bimodal with the switch to bimodality occurring at between 7 and 8 s. The bidirectionality of the shorter seas is shown to fit the hypothesis that waves are being totally reflected. Again the force density spectra—in this case both for normal and shear radiation stresses, and derived from data rather than theoretical arguments—are a significant part of the balance of forces at the margin of the ice band.

Ice bands, streamers, and other ice edge features received attention during the early 1980s, as their genesis was unknown. Notable in the present context are two studies: an experimental project done in the Bering Sea by Seelye Martin and coworkers (Martin et al 1983) and a convincing thought-experiment reported by Wadhams (1983), which is tested on an example MIZ. Both studies rest on radiation stress arguments to reach their conclusion.

There are many ways in which a wave field influences (some would say determines) MIZ morphology, but waves do not act in isolation and other factors also play a role. Using SAR imagery, the spatial variability of the wave and current fields can be estimated through spectral analysis and wave modeling. Surface effects induced by wave-current interaction and atmospheric instability may then be used to interpret mesoscale features

such as eddies and fronts in, for example, *Seasat* and *ERS-1* SAR images. Thus, based on SAR-observed wave, current, and wind inputs, a two-dimensional, coupled, ocean-ice interaction numerical model can be used, in principle, to predict the ice edge and ocean dynamics.

As an example we refer again to the LIMEX experiment. During LIMEX'87 (Carsey et al 1989) effects on ice edge meandering were observed in SAR photo mosaic coverages of southeast Newfoundland between March 21/23 and March 26, 1987 as shown in Figures 9a and 9b, respectively. The ice edge is indicated by the dashed curve and the extent of wave penetration by the dotted curve. On March 23, ocean swell was observed coming from the northeast and starting to penetrate the ice pack, as shown in Figure 9a with its relatively smooth ice edge. On March 26, because of strong easterly winds and swell, the ice was heavily compacted against the coast. Ocean swell had penetrated the entire pack to the shore. Ice edge meandering with eddies is thought to be due to wind and wave actions.

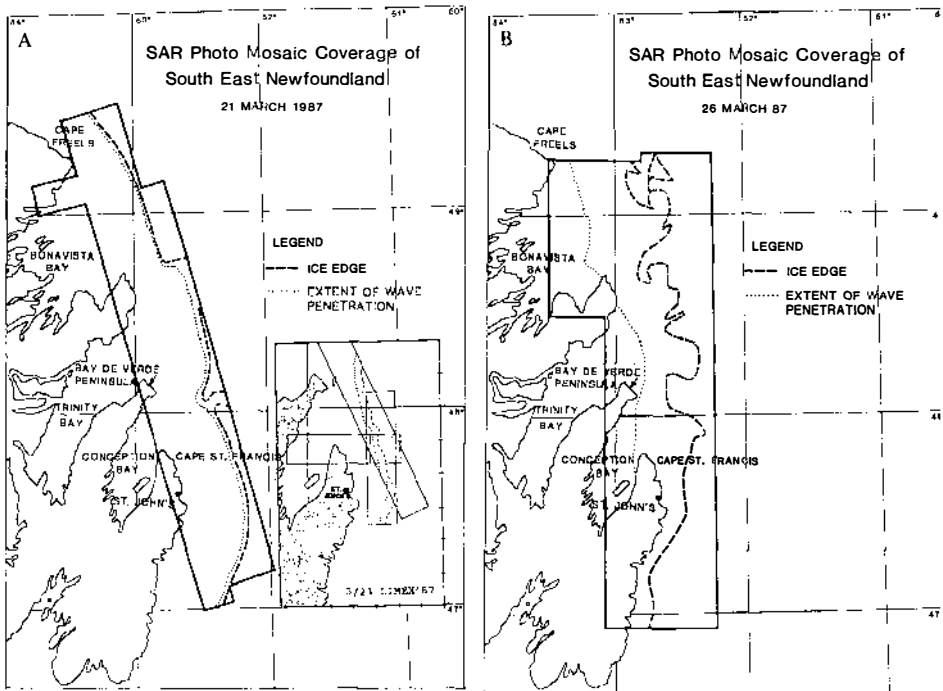


Figure 9 SAR photo mosaic coverage of southeast Newfoundland on (a) March 21 and 23, and (b) March 26, 1987 indicating the ice edge and extent of wave penetration. After Liu et al (1993).

As demonstrated by Kobayashi & Frankenstein (1987) and as is evident from above, the mean wave drift force should be included when predicting ice floe movement. Yet existing coupled, ocean-ice interaction numerical models (e.g. Gammelsrød et al 1975; Clarke 1978; Niebauer 1982; Røed & O'Brien 1983; Ikeda 1985, 1989; Hakkinen 1986, 1987; Tang & Ikeda 1989) drive the ice-edge dynamics by wind forcing alone. The MIZ model of Hakkinen (1986) has now been extended to include wave effects as well as wind stress (Liu et al 1993). For typical MIZ ice concentrations, the main dynamical balance in the ice medium is among the water-ice stress, the wind stress, and wave radiation stresses. A parametric study has been performed to compare the effects of wave and wind stress on ice-edge dynamics by considering the momentum exchange between waves and ice pack through radiation stress for decaying waves. To demonstrate the wave effects on upwelling, a numerical result from Liu et al (1993) is shown in Figure 10. The figure shows (a) ice concentrations and (b) the pycnocline change after 2 days of combined wave and favorable wind forcing. The off-ice wind is  $8 \text{ m s}^{-1}$  and inclined  $30^\circ$  from the ice edge; the waves are propagating from  $-45^\circ$  with a wavelength of 200 m. Note that the ice edge is sharp and compact because of wave action, and that the pycnocline anomaly is amplified significantly with a maximum upwelling of 11 m as compared to 4 m for wind forcing only. Upwelling at the ice edge and eddy formation are enhanced due to the nonlinear effects of wave action; wave action sharpens the ice edge and produces ice meandering, which enhances local Ekman pumping, pycnocline anomalies, and cyclonic eddy formation. Note also that jets can arise within the ice cover and near the ice edge due to the wave action; these have often been observed. This has a corollary, namely that these jets are formed along the preferential wave field nearly independently of the (weak) wind field, as observed by Nikolayev (1973).

## 2.7 *Ambient Noise*

Underwater noise is largely the result of processes occurring at the ocean surface. An ice cover on the surface inhibits some noise generating mechanisms and introduces others, and also modifies the acoustic propagation environment in the ocean. Ambient noise in polar regions is consequently very different from that found in the temperate oceans. [See Dyer (1983) for a representative spectrum.] Except for some initial measurements by Greene & Buck (1964), there have been no comprehensive comparisons between acoustic pressure in the water and the ice motions. The subject is of relevance to MIZ dynamics because many of the processes occurring in the MIZ result in the generation of ocean noise. Measurements of ocean

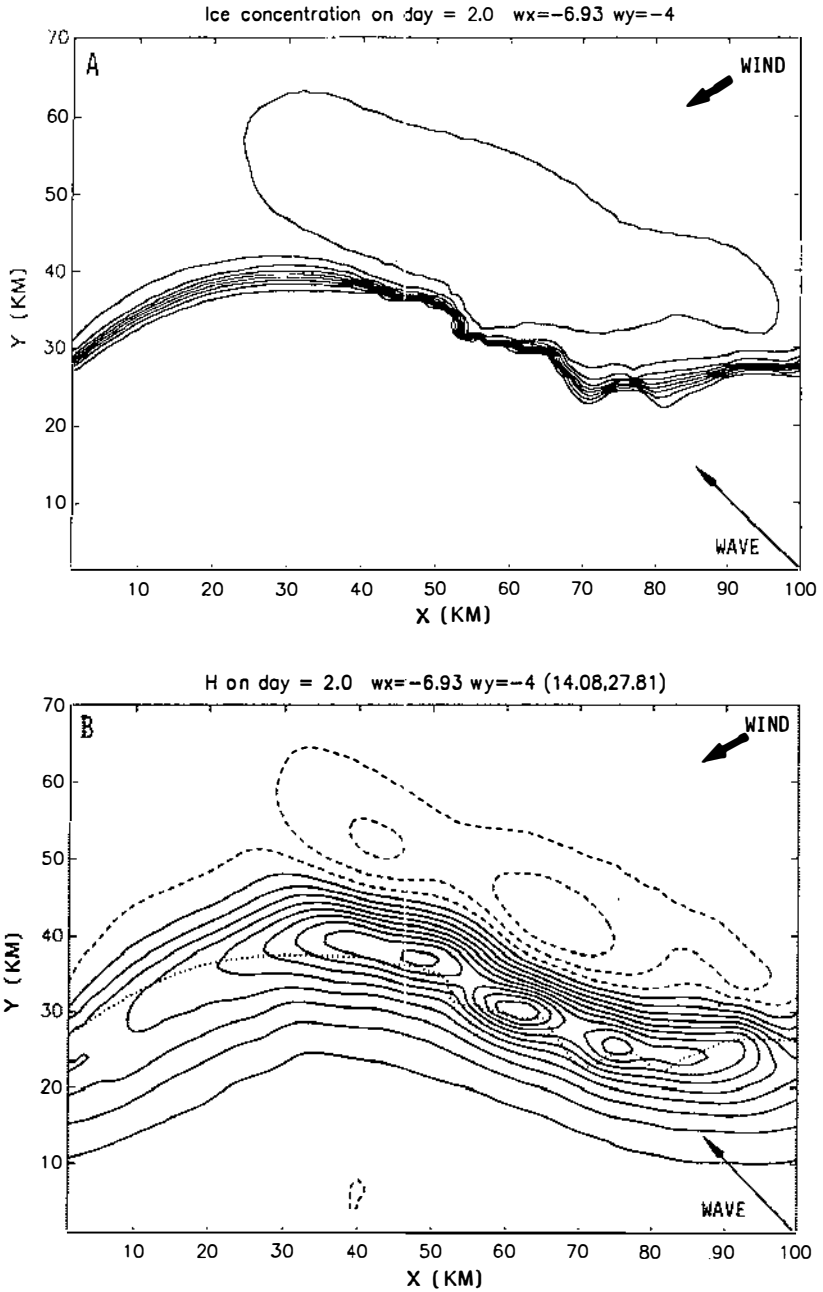


Figure 10 (a) Ice concentration and (b) pycnocline change after 2 days of combined wave and favorable wind forcing. After Liu et al (1993).

Annu. Rev. Fluid Mech. 1995.27:115-168. Downloaded from arjournals.annualreviews.org by U.S. Geological Survey - Multi-Site on 07/21/10. For personal use only.

noise combined with an understanding of the generating mechanisms may provide a convenient diagnostic tool in the investigation of MIZ processes.

A number of measurements of underwater sound levels have been made in the vicinity of the MIZ. Diachok & Winokur (1973) considered the spatial variability of ocean noise levels, observing a peak coincident with the ice edge between 100 and 1000 Hz that was more pronounced for a compact ice edge. More noise was generated in higher wind or higher sea state conditions. They concluded that the ice edge acts as a line source of noise and suggested that the predominant mechanisms responsible for noise generation were related to wave-ice interactions. Additional measurements of spatial variations in noise levels by Yang et al (1987) suggest that the ice edge cannot be considered simply as a uniform line source: "Hot-spots" with dimensions of less than 5 km, a nominal separation of about 50 km, and a lifetime of approximately one day were identified. The hot-spots are possibly related to ice edge eddies. A host of viable noise generating mechanisms are suggested: wave-induced flexing and breaking of large floes as they are advected towards open water; wave-induced crushing and chipping between adjacent floes; cavitation due to melting at the ice edge; localized ice stress increases due to winds and currents; thermal cracking; and finally, noise produced by marine life in areas of upwelling.

To identify which candidates generate ocean noise in significant quantities it is necessary to measure noise levels while simultaneously quantifying potential mechanisms. Correlation can be done either in a temporal or spatial sense, or both. It was found in the central Arctic, for example, that when the ice surface cools, either due to the passage of a meteorological front or the loss of insolation, it contracts and cracks sporadically in a sound reminiscent of popping corn. The sound waves that are generated propagate in the ice and into the water, and the spectrum averaged over many events exhibits a peak in the 10–100 Hz band (Ganton & Milne 1965, Milne 1972). In addition, if the wind blows harder than  $\geq 4 \text{ m s}^{-1}$ , it picks up ice crystals from the surface which make a "hissing" noise as they blow across the surface (Ganton & Milne 1965, Milne 1974). More recently, Makris & Dyer (1986) have identified two composite measures of the stress applied to an ice sheet by the combined action of wind, current, and drift in the central Arctic, which are highly correlated with variations in 10–20 Hz ambient noise levels on time scales in excess of one hour. They conclude that noise production increases with the environmentally-induced stress state within the ice. Near the ice edge the same authors (Makris & Dyer 1991) found that the best correlate was the surface gravity wave amplitude for periods  $\geq 8 \text{ s}$ . They also observed episodes of high noise levels occurring at times of low surface wave activity and

suggested that these were driven by off-ice winds or internal waves. Johannessen et al (1990) show that ambient noise levels increase when swell is present, but they also find a correlation between increased noise levels and the presence of ocean eddies. Clearly, a number of environmental driving forces—such as ocean swell and ice-edge eddies—are important to noise generation in the MIZ while being of less significance in the central Arctic.

Noise generation by floe collisions was treated by Rottier (1991) in a model in which the noise level is related to a collision rate that depends on ice concentration, floe size, and the presence or absence of brash ice between larger floes. Supporting concurrent ambient noise and wave spectrum data were acquired during MIZEX-87 (Marginal Ice Zone Experiment) and SIZEX (Seasonal Ice Zone Experiment). There is considerable promise in this kind of approach, since if the noise is induced by collisions, and if a valid treatment of collision rates can be developed in terms of the wave field and ice floe sizes, then in situ data should yield the empirical factor relating collision rates to noise, giving a predictive capability.

### 3. OCEAN WAVES AND CONTINUOUS SEA ICE

We now turn to the other major ice type of the polar and sub-polar seas, namely the continuous ice sheet. Here we consider the majority of the sea ice found within the Arctic Basin where—rather than the ice cover being composed of a distribution of sizes of individual ice floes floating freely in open sea at some concentration—the ice is essentially continuous with the relief broken only by the occasional lead or pressure ridge. We include the coherent sheets of sea ice that form in bays and harbors and along the coastline of the Arctic and Antarctic landmasses, and often linger after the pack ice has departed in the spring. We also consider the vast floes beyond the MIZ or perhaps embedded within it. Waves penetrating such an ice canopy may travel great distances and have been recorded throughout the Arctic Ocean (Hunkins 1962). The little attenuation they do experience comes from the (slight) hysteresis during flexure, viscous losses in the water boundary layer, and reflection from features such as cracks, leads, and pressure ridges within the sheet.

The first attempt to model theoretically wave propagation within a continuous ice sheet is due to Greenhill (1887, 1916) who considered an elastic beam floating on water of finite depth. This work really set the scene for all subsequent theoretical development on the topic; he was the first to show, for example, that ice-coupled waves disperse in a different manner from surface gravity waves in open water. Ewing et al (1934), Ewing & Cray (1934), and later Press et al (1951), Press & Ewing (1951),

and Oliver et al (1954), developed Greenhill's ideas further in a series of seismic field experiments and analyses to study elastic and flexural ice-coupled wave propagation in ice of various types, including the compressibility of the water column and treating the ice as a plate rather than as a beam. The waves in the field experiments were generated artificially in a frozen canal by detonation and were used to measure the high frequency Young's modulus of ice. Roethlisberger (1972) summarizes this program of seismic work.

### 3.1 Propagation in Continuous Ice

Waves in a continuous sheet of sea ice floating on an infinite depth of water are usually considered to disperse according to

$$L\kappa^5 + (\rho g - \rho' h \omega^2)\kappa - \rho \omega^2 = 0, \tag{27}$$

where Equation (4) and the thin elastic plate surface condition (5) have been used, assuming a wave mode proportional to  $e^{i(\kappa x - \omega t)} e^{-kz}$ . The thick elastic plate has also been considered (Fox & Squire 1991a). The mass-loading model, which simply neglects  $L$  in Equation (27) (Squire 1993b), does not reproduce observations in continuous ice sheets well, as ice sheets do appear to possess elasticity. The roots of this fifth-order polynomial must be found numerically; they comprise a single principal root corresponding to an undamped traveling (flexural-gravity) wave, together with two complex conjugate pairs of roots with each root corresponding to a damped-traveling wave.

In Figure 11 the principal wavelength in the ice is plotted against wave

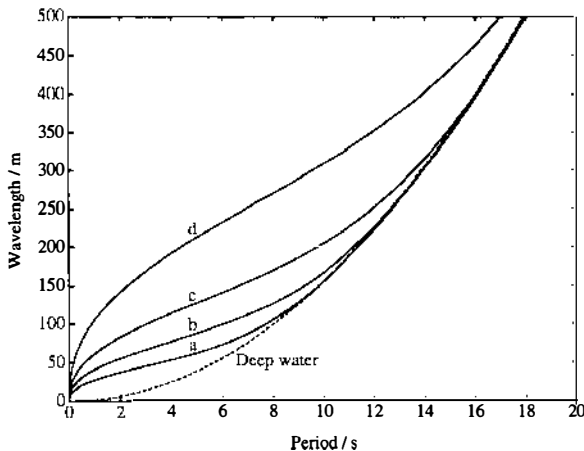


Figure 11 Deep-water, ice-coupled flexural-gravity wavelength (solid curves) as a function of wave period for ice thicknesses of (a) 0.5 m, (b) 1.0 m, (c) 2.0 m, and (d) 5.0 m. The equivalent open water curve is also plotted (dashed).

period for several ice thicknesses, alongside the equivalent (deep) open water curve. The wavelength is always greater than that in open water, and at a particular period is greatest for the thickest ice sheet, though the curves coalesce at long periods. The corresponding curves for a mass-loading model (not plotted) would lie beneath the open water curve as in this case wavelength always decreases on entering the ice. Phase and group velocity curves are shown in Figure 12. The phase velocity curves each decrease to a minimum—through which their group velocity partner must pass—and then increase monotonically to the deep open water phase velocity asymptote, which is linearly proportional to wave period. To the left of the minimum is the flexural branch, where dispersion is described mostly by the nature of the bending ice, and to its right the dispersion is described mainly by the hydrodynamics; hence the term flexural-gravity wave. The phase velocity minimum moves towards higher period as thickness is increased as would be expected, since waves of a specific period will feel the effect of thicker ice to a greater extent than thinner ice.

Because the flexural-gravity wave number is real for purely elastic ice, the wave as modeled experiences no attenuation as it travels through the ice. In reality, energy is gradually lost from the wave and as a result it systematically attenuates with distance covered. Observations suggest that damping is roughly exponential at any one wave period and that the attenuation coefficient decreases as period increases. Two approaches have been used to model this energy loss. Wadhams (1973b) assumed that the propagation is governed by (27), but that during each cycle the ice suffers

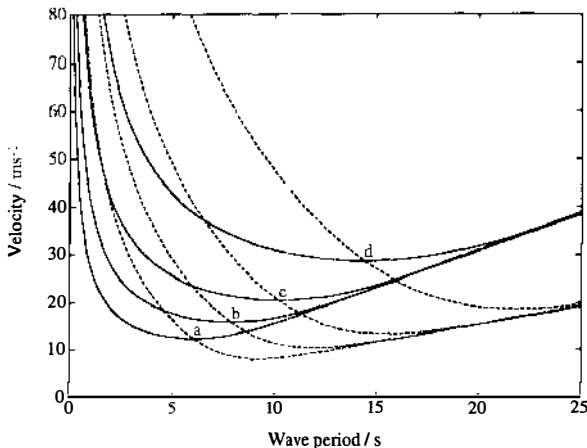


Figure 12 Dispersion of flexural-gravity waves in an ice sheet at various thicknesses on infinite water depth. The solid curves represent phase velocity ( $\omega/k$ ) and the dashed curves group velocity ( $d\omega/dk$ ), for ice thicknesses of (a) 0.5 m, (b) 1 m, (c) 2 m, and (d) 5 m.

a hysteresis loss due to Norton creep. The second approach uses a different ice rheology (commonly linear viscoelasticity) and modifies Equation (27) accordingly, either by means of the correspondence principle (Squire 1978, Squire & Allan 1980, Bates & Shapiro 1980), by a velocity-dependent damping term (Squire & Fox 1992), or from first principles (Squire 1978, 1984b).

### 3.2 *The Edge of an Ice Sheet*

Ocean waves entering a region covered by a continuous ice sheet are only partially transmitted at the margin; a proportion of the incoming energy is reflected back into the open sea. Within the ice various wave modes are created: a propagating flexural-gravity mode which may travel far into the ice sheet; a pair of heavily-damped propagating modes which are limited to the vicinity of the ice margin itself; and—for finite water depth—an infinite number of evanescent (Budden 1988) ice-coupled wave modes which correspond to the imaginary roots of the dispersion relation. An equivalent set of evanescent modes are created in the open water by the reflection process. For infinite water depth, evanescent modes relate to the continuous spectral solution. Waves propagating into an ice sheet lead to a complicated wave structure, which was not solved precisely until the early 1990s (Fox & Squire 1990, 1991b, 1994).

The first attempt to model wave penetration into sea ice was made by Hendrickson & Webb (1963) (see also Wadhams 1986). Like the earlier finite-floe model due to Wadhams (Section 2) only an approximate solution was achieved at this time, as the evanescent wave modes were not included in full. Squire (1978, 1984a,b,c,d) developed the method further, considering more sophisticated dispersion relations that included the physical properties of sea ice in a more realistic manner. The inherent hydrodynamic approximation, whereby the velocity potential corresponding to the evanescent modes was omitted, was not addressed. A formal mathematical solution to the problem was reported by Evans & Davies (1968) but, while extremely valuable in setting up the problem, the method used did not allow solution except in the shallow water limit.

The aim throughout has been to synthesize observations of waves penetrating ice sheets and their dispersion and attenuation in the ice. The breakup of shore fast ice in harbors and embayments is often wave-induced, in which case the regularity of the ice structures created is tantalizing. The Fox & Squire (1990, 1991b, 1994) theories essentially solve most of the outstanding facets of the problem and go a long way towards explaining many of our observations.

THE FOX & SQUIRE MODEL Here we outline the mathematical model of

Fox & Squire (1994), derived to describe small-amplitude ocean waves propagating obliquely from the open sea into a floating ice sheet. In the small-amplitude limit the differential equations are linear, allowing superposition techniques to be used. The simplest case of single frequency, and hence steady state, excitation is considered. The solution for more complicated types of excitation, such as an incoming directional wave spectrum, can be found by superposing solutions of the simpler system.

A semi-infinite ice sheet of thickness  $h$  floats at the surface of water of constant depth  $H$  (Figure 13). The ice sheet floats on the water surface in the semi-infinite region  $0 \leq x < \infty$ ,  $y = H$ ,  $-\infty < z < \infty$ . Note that this coordinate system is defined differently from that used in Section 2 following Fox & Squire (1994). The boundary value problem is then

$$\nabla^2 \Phi = 0, \quad (28)$$

$$\left. \frac{\partial \Phi}{\partial y} \right|_{y=0} = 0, \quad (29)$$

$$\frac{\partial^2 \Phi}{\partial t^2} = -g \frac{\partial \Phi}{\partial y}, \quad -\infty < x < 0, \quad y = H, \quad (30)$$

$$\left( I \nabla_{xz}^4 + \rho' h \frac{\partial^2}{\partial t^2} + \rho g \right) \frac{\partial \Phi}{\partial y} + \rho \frac{\partial^2 \Phi}{\partial t^2} = 0, \quad y = H, \quad 0 \leq x < \infty, \quad (31)$$

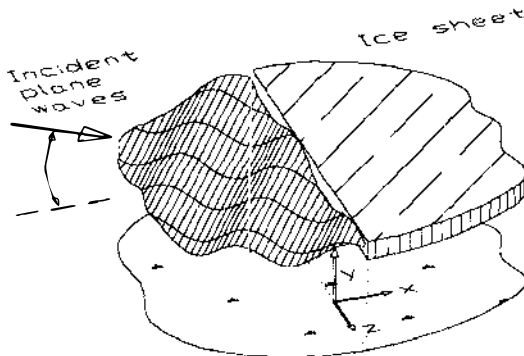


Figure 13 Plane ocean waves obliquely incident on a sheet of shore fast sea ice. The coordinate system used in the model is located on the sea floor beneath the ice edge as shown. After Fox & Squire (1994).

$$L \frac{\partial^2}{\partial x \partial y} \nabla_{xz}^2 \Phi + (1 - \mu)L\Phi_{xyz} = 0, \tag{32}$$

$$x = 0^+, \quad y = H, \quad -\infty < z < \infty,$$

$$L(\Phi_{xxy} + \mu\Phi_{yzz}) = 0, \quad x = 0^+, \quad y = H, \quad -\infty < z < \infty. \tag{33}$$

Equations (32–33) are the oblique generalization of Equation (8). With  $\Phi(x, y, z, t) = \phi(x, y)e^{i\omega t}e^{ik_z z}$ , system (28)–(33) becomes the well-defined, classical boundary value problem which is solved variationally by Fox & Squire (1994) to an arbitrarily prescribed precision:

$$\left( \frac{\partial^2}{\partial x^2} + \frac{\partial^2}{\partial y^2} - k_z^2 \right) \phi = 0, \quad -\infty < x < \infty, \quad 0 < y \leq H, \tag{34}$$

$$\frac{\partial \phi}{\partial y} = 0, \quad -\infty < x < \infty, \quad y = 0, \tag{35}$$

$$g \frac{\partial \phi}{\partial y} - \omega^2 \phi = 0, \quad -\infty < x < 0, \quad y = H, \tag{36}$$

$$\left[ L \left( \frac{\partial^2}{\partial x^2} - k_z^2 \right)^2 - \rho' h \omega^2 + \rho g \right] \frac{\partial \phi}{\partial y} - \rho \omega^2 \phi = 0, \quad 0 < x < \infty, \quad y = H, \tag{37}$$

$$\left[ \frac{\partial^3}{\partial x^3} - (2 - \mu)k_z^2 \frac{\partial}{\partial x} \right] \frac{\partial \phi}{\partial y} = 0, \quad x = 0^+, \quad y = H, \tag{38}$$

$$\left( \frac{\partial^2}{\partial x^2} - \mu k_z^2 \right) \frac{\partial \phi}{\partial y} = 0, \quad x = 0^+, \quad y = H. \tag{39}$$

In the open sea region,  $-\infty < x < 0$ , the bounded solution is

$$\phi_1 = (Ie^{-ik_T x} + Re^{ik_T x}) \cosh k_T y + \sum_{n=1}^{\infty} a_n e^{k_n' x} \cos k_n' y, \tag{40}$$

where  $I$  and  $R$  are the complex coefficients of the traveling (denoted by the subscript T) waves,  $\{a_n\}$  is the set of coefficients of the bounded evanescent modes, and  $k_T' = \sqrt{k_T^2 - k_z^2}$  and  $k_n' = \sqrt{k_n^2 + k_z^2}$ . The quantities  $\pm ik_T$  and  $\pm k_n$  are respectively the imaginary and real roots of the open water dispersion relation

$$k \tan kH = -\frac{\omega^2}{g}, \tag{41}$$

derived from Equation (36).

In the ice-covered region,  $0 \leq x < \infty$ ,  $k$  is replaced by  $\kappa$  to distinguish between the two regions.  $\kappa$  must satisfy

$$\kappa \tan \kappa H = -\frac{\rho\omega^2}{L\kappa^4 - m\omega^2 + \rho g}. \tag{42}$$

This dispersion equation also has two imaginary roots  $\pm i\kappa_T$  corresponding to traveling waves, four complex roots  $\pm \kappa_D$  and  $\pm \kappa_D^*$  corresponding to damped (or growing) traveling waves, and infinitely many real roots  $\pm \kappa_n$ , each giving an evanescent (or growing) mode. The bounded solution for the ice-covered region,  $x > 0$ , is then

$$\begin{aligned} \phi_2 = & T e^{-i\kappa_T x} \cosh \kappa_T y + b_+ e^{-\kappa_D x} \cos \kappa_D y + b_- e^{-\kappa_D^* x} \cos \kappa_D^* y \\ & + \sum_{n=1}^{\infty} b_n e^{-\kappa_n x} \cos \kappa_n y, \end{aligned} \tag{43}$$

where  $T$ ,  $b_+$ ,  $b_-$ , and  $\{b_n\}$  are the complex coefficients of the various modes, and  $\kappa_T' = \sqrt{\kappa_T^2 - k_z^2}$ ,  $\kappa_D' = \sqrt{\kappa_D^2 - k_z^2}$ , and  $\kappa_n' = \sqrt{\kappa_n^2 + k_z^2}$ . In this case it is possible for either  $k_z < \kappa_T$  or  $k_z \geq \kappa_T$ . In the former case  $\kappa_T'$  is real and the principal traveling mode suffers no attenuation; in the latter case  $\kappa_T'$  is pure imaginary and the mode becomes evanescent, corresponding to a critical incidence angle and total reflection of the incoming wave.

The solution is found by minimizing

$$\varepsilon = \int_0^H |\phi_2 - \phi_1|^2 dy + \gamma \int_0^H \left| \frac{\partial \phi_2}{\partial x} - \frac{\partial \phi_1}{\partial x} \right|^2 dy, \tag{44}$$

while satisfying the ice edge boundary conditions (38–39) and an additional condition that sets the incoming wave's displacement to unit amplitude. The constant  $\gamma$  is a weighting term included to improve convergence.

The  $z$ -components of the open water wave number  $k_T$  and its counterpart in the ice  $\kappa_T$  are equal. Hence

$$k_T \sin \theta_1 = \kappa_T \sin \theta_2, \tag{45}$$

where (41) and (42) give the wave numbers  $k_T$  and  $\kappa_T$ , and  $\theta_1$  and  $\theta_2$  are the angles of incidence and transmission, respectively. If  $k_T < \kappa_T$ , the transmitted traveling wave is refracted towards the normal at the ice edge, but if  $k_T > \kappa_T$  it is refracted away. The former case only occurs when the wave numbers are very small and more commonly  $90^\circ \geq \theta_2 > \theta_1$  (see

Figure 11). When  $\theta_2 = 90^\circ$ ,  $\theta_1 = \sin^{-1}(\kappa_T/k_T)$ , thereby defining a critical angle for waves entering the ice sheet (Figure 14).

The critical angle curve is drawn dotted in Figure 15, which shows the complex behavior of the reflection coefficient as a function of both period and incident angle. An equivalent figure for deep water has a very similar structure, while that for shallow water is rather different (see Fox & Squire 1994).

Some consequences of the reflection of incoming surface waves from a sheet of sea ice were investigated by Squire & Fox (1990). For mono-

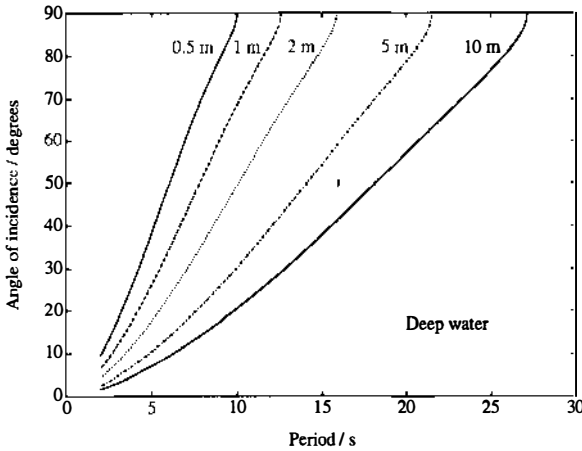


Figure 14 Critical angle curves at various thicknesses for deep water. After Fox & Squire (1994).

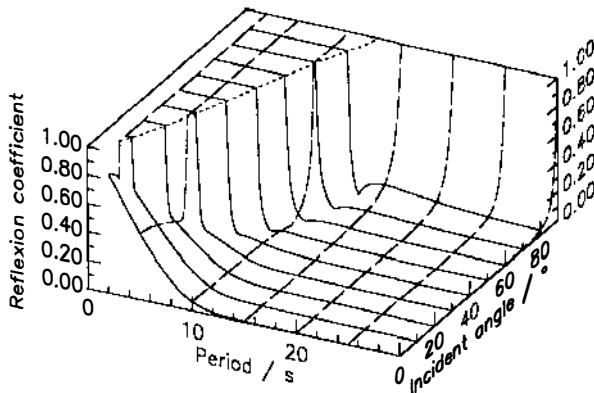


Figure 15 Three-dimensional plot showing the variation of reflection coefficient with angle of incidence and wave period for 1 m thick sea ice on a water depth of 100 m. After Fox & Squire (1994).

chromatic waves the sea takes on a corrugated appearance when  $R$  is a significant fraction of unity, i.e. particularly for thick ice or short period waves. Because  $R$  varies strongly with frequency, spectral densities created by an incoming surface wave spectrum are very complex due to interference.

**BREAKUP** Ocean waves have been observed by many researchers to break up sheets of shore fast ice. Indeed, one of the authors (VAS) has been privileged to witness breakup on several occasions, in some cases nearly losing instruments and snowmobiles, and in all cases destroying a carefully planned set of experiments before we were ready to begin. Despite this, the mechanism by which breakup occurs is poorly understood. Anecdotally it appears that incoming waves and swell cause a fracture line to develop a few tens of meters back from the ice margin and parallel to it. Almost instantaneously, the fracture opens up and the strip of ice floats clear. Since this has negligible effect on the incident sea, there is effectively now a new ice edge which is subjected to the full force of the incoming waves and a fracture forms in a similar fashion to create a second strip of ice. Eventually the entire ice sheet breaks up into a series of parallel strips which subsequently fracture into angular floes along their length. The width of the strips, and hence the diameter of the floes created by the process, is remarkably consistent and appears in the sparse evidence available to be rather insensitive to the spectral structure of the sea but highly dependent on ice thickness.

Squire (1984a,c,d) attempted to explain wave breakup of shore fast ice in terms of the pair of damped-traveling waves generated at the ice edge, either at normal incidence or otherwise, and especially when incidence is supercritical. This interpretation has been superseded by the Fox & Squire (1990, 1991b, 1994) work. At normal incidence the later theory gives a strain envelope rising from zero at the free edge to its asymptotic value after the evanescent and damped-traveling waves have died away. In between, it may attain a maximum a few tens of meters from the ice edge. Using the sea ice fracture strains reported earlier (Goodman et al 1980, Squire & Martin 1980) we may directly scale the incident wave amplitude to produce a particular strain value at some point, say its maximum value, to give a rough idea of the open water wave amplitude required to produce breakup. For 1 m of ice, waves in the broad 5–10 s range will break the ice if their amplitude is 90 mm or more, whereas a 15 s wave would require an amplitude of 280 mm and a 20 s wave would need an amplitude of 630 mm. Waves of 25 s period and beyond require amplitudes of greater than 1 m to break the ice.

The strain generated within the ice sheet due to obliquely incident waves

is complicated, and the reader is referred to Fox & Squire (1994). Principal strains must be computed for the combined set of wave modes penetrating the ice, and these will change through the wave cycle.

The most recent model of breakup fits observations well (Squire 1993a). Using a variation on the Fox & Squire method, Squire considers wave propagation into a viscoelastic ice sheet and computes the strain magnitude envelope back from the ice edge for various wave periods (Figure 16). In each case the strain envelope is zero at the ice edge, increases to a maximum a certain distance in (26.0 m, 38.5 m, 40.0 m, 40.5 m, 40.5 m, for increasing period), and then decreases exponentially due to damping. In Figure 16 note that the penetration at which maximum strain occurs is quite insensitive to wave period. By taking the locus of maximum strains, described by choosing all wave periods between 2 s and 25 s at a constant incident amplitude of 1 m, it is shown that even the long 25 s period waves produce their largest strain at only about 40 m penetration; shorter waves give maximum strains even closer to the ice edge. The loci of maximum strain, taken between 2 and 25 s as before for four ice thicknesses, are shown in Figure 17. Each curve is displaced towards greater penetration as thickness is increased, and each is bounded on the right so that fracture cannot occur beyond a certain distance into the sheet irrespective of wave amplitude. The 0.5 m curve is bounded at about 40 m, the 1 m curve at 69 m, and the

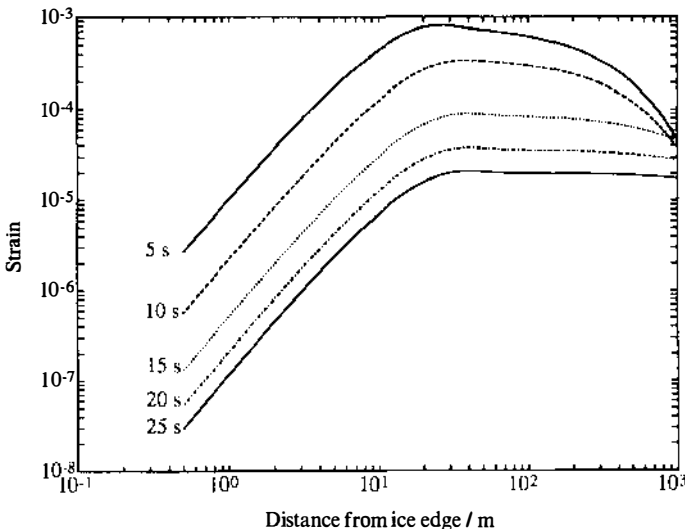


Figure 16 The strain envelope due to the ice-coupled wave field plotted against penetration into the sea ice sheet for wave periods of 5, 10, 15, 20, and 25 s. Ice thickness is 0.5 m; water depth is 100 m. After Squire (1993a).

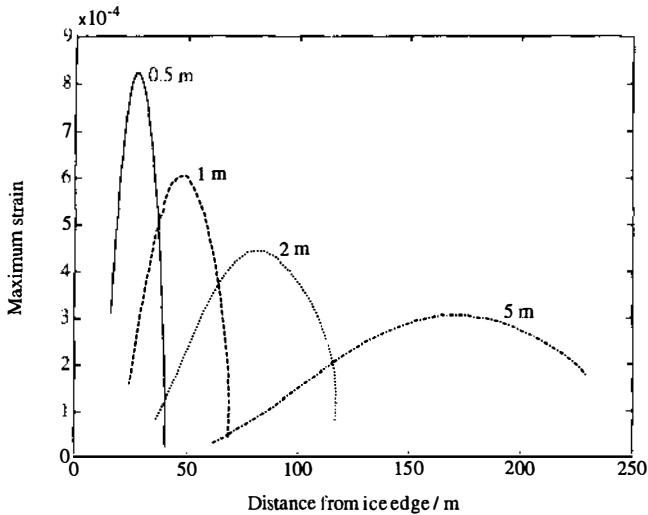


Figure 17 Plot of maximum strain vs penetration at ice thicknesses of 0.5 m, 1 m, 2 m, and 5 m. The greatest strain attained for 0.5 m ice is at a penetration of 27.7 m by a 5.5 s period wave, 47.9 m for 7.25 s in 1 m of ice, 81.5 m for 9.5 s in 2 m of ice, and 170.9 m for 14.5 s in 5 m of ice. After Squire (1993a).

2 m curve at 117 m. The 5 m curve is not bounded in the 2–25 s range. Each locus peaks at a value that corresponds to the wave period most likely to cause cracks to develop. In all cases the strain magnitudes are quite sufficient to fracture the sea ice, taken in the context of our initial assumption that the incoming wave has an amplitude of 1 m.

Although these results are derived for waves incident on a continuous ice sheet, they may have relevance to large floes in the MIZ. Then the distances given in Figure 17 would define “typical” diameters for floes of various thicknesses in the MIZ. A test of this idea would be to see whether floe size distributions in the Bering, Labrador, and Greenland Seas show peaks at different diameters, based on the differences in typical ice thicknesses among these three seas; anecdotal evidence suggests that this is indeed the case.

**A SECOND-ORDER MODEL** The normal incidence models of Fox & Squire (1990, 1991b) have been extended to second order by Fox (1992) using a Stokes expansion. It is found that the second-order terms within the water have an approximately 1% effect for a 5 s wave of 40 mm amplitude, and a 10% effect at 0.4 m. Longer period waves have less effect as they are less steep. Within the ice, the second-order terms for a 5 s wave have less than a 1% effect on the displacements for incident amplitudes of 0.1 m. Strain is slightly more dependent on second-order effects than is displacement.

**OBSERVATIONS** Very few articles in the literature present measurements on wave penetration into an ice sheet, mainly because it is notoriously difficult to collect such data. An early strain gauge experiment in Newfoundland (Squire & Allan 1980) verified dispersion relation (27). Later, accelerometers were used in a serendipitous experiment on fast ice in north Spitzbergen to determine the dispersion and damping suffered by the principal ice-coupled wave (Squire 1984b). The large attenuation coefficients found were believed to be due to the high brine volumes recorded for the ice sheet. Two models were successfully applied to these data: Squire (1984b) proposes a temperature-dependent (thermorheologically simple) thin plate model; whereas Squire & Fox (1992) invoke the thin plate equation of Robinson & Palmer (1990) with variable  $E(z)$ . Most recently, a successful project utilizing a sea state radar to measure the waves off the ice edge and many strain gauges on the ice sheet has been conducted in McMurdo Sound, Antarctica (Squire et al 1994).

### 3.3 *Waves in the Central Arctic*

Sea ice in the Arctic Ocean exhibits vibrational motions across a wide band of frequencies. The ice moves vertically and horizontally in response to many different types of physical forcing mechanisms, some that have been clearly identified in measurements and some that remain hypothetical. To date, observations of these motions have been made with several types of instruments, for many different purposes, at widely scattered locations and times, with little attempt to compare results and to identify uniquely the processes responsible. As a result, there presently is no widely accepted model for these motions that is valid across the broad band of frequencies measured to date.

The construction of an empirical model of the motion spectrum is a useful step in identifying the dominant processes that cause the motions. Given measured spectra, the important physical processes can often be identified by one or more of several well-known procedures. One successful procedure has been to study significant features in the spectra, e.g. local peaks, changes in slope, spectral gaps between two frequency bands, noting especially features that change with external circumstances. Association of spectral changes with changes in the environmental circumstances in which they were observed allows hypotheses to be made about the physical processes that cause the motions (e.g. DiMarco et al 1991).

The spectral model is also an important research tool as it often permits predictions to be made for physical quantities that have not yet been directly measured, and it enables comparisons to be made between data sets acquired from different instruments.

**THE PHYSICAL MECHANISMS** Very low frequency vertical motions of sea ice ( $< 10^{-4}$  Hz) are due to all forces that cause the ocean surface to rise and fall, including barotropic and baroclinic tides, atmospheric synoptic pressure changes, and mesoscale motions associated with eddies and fronts in the ocean. Since the length scales are very long ( $\geq$  tens of km) the ice simply replicates the vertical motion of the water surface.

Low frequency motions due to inertial-internal gravity waves occur in the band from the inertial frequency to the maximum buoyancy frequency (say  $2.5 \times 10^{-5}$ – $2 \times 10^{-3}$  Hz). At long horizontal wavelengths the surface continues to follow the hydrostatic surface elevation; the response is reduced for shorter wavelengths. The wavelength at which the response falls off relative to an ice-free surface relates to simple physical effects. First, the ocean mixed layer (typically  $\geq 30$  m deep) beneath the ice exponentially attenuates the pressure field associated with internal waves propagating in the pycnocline so that waves shorter than  $\sim 100$  m do not provide sufficient pressure fluctuations to affect the ice. Second, because of the bending stiffness of the ice, wavelengths shorter than  $2\pi l = 2\pi(L/\rho g)^{1/4}$ , where  $l$  is the characteristic length, are inhibited.

Because of attenuation the only surface gravity waves in the central Arctic are those at very low frequency ( $< 0.05$  Hz) or those generated locally by wind. Low frequency swell has been observed practically every where, apparently; Fram Strait is a common source during all seasons.

The wind may also cause appreciable ice motions in a frequency band near 0.1 Hz due to: (a) pressure fluctuations in the atmospheric boundary layer which move the surface hydrostatically or quasi-statically (DiMarco et al 1991); and (b) pressure fluctuations that resonantly generate surface waves (Davys et al 1985) in a manner fully equivalent to the Phillips (1957) mechanism on open water.

Flexural-gravity waves in the 0.1–10 Hz band are probably generated by interactions between adjacent floes, especially during pressure ridging events. Although dissipated quickly, they usually are so large in amplitude during active ridging that they are easily detectable. However, they do not travel easily from one floe to the next.

Narrow-band, high energy motions with durations of up to many minutes and  $\sim 1$  Hz frequencies have been observed (Bogorodskiy & Smirnov 1982). These are hypothesized to be associated with interactions between adjacent floes, perhaps rafting of thinner ice during compression or lateral motions of adjacent floes that are under simultaneous compression and shear.

Ridging events also generate noise in the water (Greene & Buck 1964, Buck & Wilson 1986). Unless the water depth is shallow, this sound arrives on surrounding floes because of the typical upward refracting

sound velocity profile in the waters beneath. Measureable vibrational motions at the surface are induced, even if the ice only acts as a boundary causing the sound to be reflected back down into the water column. Low frequency sound can travel long distances and may dominate the local energy level of motions if the instrumented floe is otherwise quiet.

Above about 10 Hz, most of the energy is acoustic in nature, having been generated by one or another of several known mechanisms. The ridging mentioned above often is a dominant source and is associated with large-scale compression or shear of the ice field (Pritchard 1984). In the water, there is an apparent low Q peak in the spectrum near 10 Hz (Makris & Dyer 1986). Additional mechanisms occur at higher frequencies (Ganton & Milne 1965; Milne 1972, 1974) as discussed earlier.

**THE MODEL VELOCITY SPECTRUM** For consistency, results are presented here in terms of vertical velocity as one of the authors (JPD) has often used geophones. Measurements previously made with other instruments, e.g. tiltmeters, accelerometers, seismometers, or strain gauges, can often be interpreted in terms of velocity. For example, measurements of surface tilt can be accomplished by using an instrument that is sensitive to horizontal acceleration (DiMarco et al 1991, Dugan et al 1992, Czipott & Podney 1989, Czipott et al 1990, Williams et al 1990), noting that actual horizontal acceleration events may cause the data to be difficult to interpret. The vertical velocity spectrum  $S_v$  is then related to the tilt spectrum  $S_\theta$  by  $S_v(\omega) = \omega^2 k^{-2} S_\theta(\omega)$ . Likewise, strain measurements can be converted to velocity or tilt if one assumes elastic bending of the ice plate and a known dispersion relation.

A composite vertical ice velocity spectrum, with curves representative of energy levels measured at different times by different types of instruments, by several different investigators, and with each curve representing a specific physical process, is given in Figure 18. Data for the frequency band 0.1–100 Hz were measured directly with vertically oriented geophones; those between 0.02 and 1 Hz were temporally integrated from accelerometer records; others were calculated theoretically. The hypothesis is that any observed spectrum is a combination of these component parts (Dugan et al 1986); each specific curve has been selected to emphasize a physical mechanism which is now discussed in more detail.

*Internal gravity waves* There is a long history associated with the hypothesis of low frequency ice motions being driven by internal gravity waves in the density-layered water below the ice. A seminal paper by Smirnov (1972) exhibited samples of data to support the hypothesis. Additional data were published in the Russian literature in the 1970s, and it has been a recurring theme of the work at the Arctic and Antarctic Research

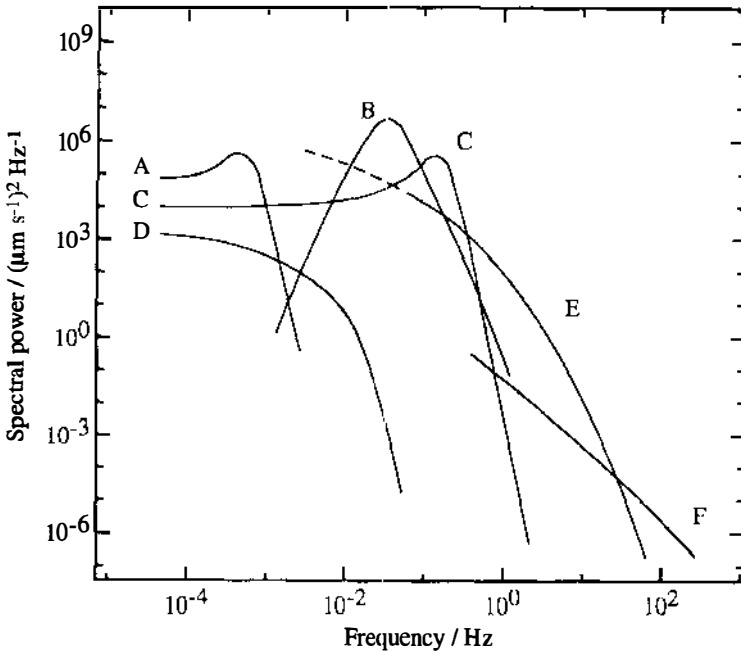


*Figure 18* Model spectrum for vertical velocity. (A) internal gravity waves, scaled from open ocean measurements; (B) surface gravity waves; (C) wind generated motions; (D) theoretical prediction for water turbulence; (E) flexural waves from pressure ridging; (F) acoustic waves. Curves B, C, E, and F are redrawn from Dugan et al (1992).

Institute (AARI) since then. Russian seismograph data suggest that the waves are very long, probably  $\geq 1$  km, that they travel great distances, that they cause inferred vertical motions of the ice 1–10 mm in amplitude, and that the wave speed is 1–2 m s<sup>-1</sup>. The wave amplitude in the pycnocline would be expected to be order 1–10 m to move the surface 1–10 mm. These observations are consistent with what is known about internal waves in the pycnocline below the ice in the Arctic Ocean (Levine et al 1985, 1987), so this interpretation of the observations appears justified.

More recently, simultaneous ice tilt and strain, and pycnocline displacement measurements near the continental shelf north of Spitzbergen during the Coordinated Eastern Arctic Experiment (Czipott et al 1989, Williams et al 1990) have been reported. A large-amplitude internal wave group was found to be traveling in a direction away from the nearest underwater topographic feature. The link between ice tilt and strain and the pycnocline makes a compelling case for the event, though more generally we remain uncertain how much energy in the ice motion is associated with internal waves.

The internal wave spectral estimate of Figure 18 (curve A) was scaled from open ocean measurements (Pinkel 1975) using the factor estimated by Levine et al (1985) for the Arctic. The signal peaks near  $10^{-3}$  Hz, is white toward lower frequencies, and rolls off at higher frequencies in accordance with Czipott & Podney (1989). The level and trend are reasonably consistent with the tilt measurements scaled to velocity units.

*Surface gravity waves* Almost all observations of ice motions in the Arctic exhibit a sharp spectral peak between 0.03 and 0.05 Hz due to swell from the open ocean. Surface gravity waves which are generated by the wind in the open ocean propagate into the ice, and all higher frequency motions are damped rapidly either within the MIZ or by hysteresis loss during ice flexure within the ice interior. Above about 0.1 Hz the flexural rigidity overwhelms gravity as the most important restoring force in the dispersion relation (Figure 12), and waves are dissipated by one or more of the hypothesized processes described earlier. Lower frequency components of the swell (order 25 s period) that are hardly apparent in open ocean measurements do not flex the ice appreciably since the waves are so long (order 1 km), and propagate with little attenuation throughout the Arctic (Hunkins 1962, Dugan et al 1992). The largest waves propagate into the ice field through Fram Strait and then spread throughout the Arctic, just as the great Antarctic swell is known to propagate throughout the more temperate oceans (Munk et al 1959).

The wave spectrum exhibits a rather high Q since it is the remainder of swell generated elsewhere. The spectrum rises steeply from the level at lower frequencies because there is little generation of swell by the wind or wave-wave interactions there, and it rolls off steeply at higher frequencies because of the dissipative mechanisms mentioned above. The level of curve B is the mean level measured by Dugan et al (1992) at 85°N above Fram Strait, with the slopes estimated from various measured spectra. They are consistent with other measurements both in frequency and amplitude, but may be expected to vary by an order of magnitude in amplitude.

*Motions due to turbulence in the wind* Locally, the wind can generate propagating surface waves, but probably only on the thinner ice of refrozen leads, and even then the waves are dissipated quickly in the surrounding (thicker) ice cover. Wind generation of waves in ice was first noted by Hunkins (1962) and studied latterly by Squire (1986) and Crocker & Wadhams (1988). The most recent theory for the mechanism causing this motion involves the turbulent eddies in the atmospheric boundary layer that are carried downwind at the mean wind speed. If this speed is anywhere near or greater than the minimum phase speed of flexural-gravity waves (see Figure 12 and Equation 27), then motions of the ice can be

generated efficiently by resonance. If the wind speed is subcritical, i.e. less than the minimum phase speed, the pressure fluctuations simply move the ice quasi-statically as they travel downwind. Spectrum C in Figure 18 is an example for a first-year, 0.5 m thick refrozen lead, where the subcritical mean wind speed was  $10 \text{ m s}^{-1}$  (Dugan et al 1992).

For subcritical motions, which occur almost all the time, the theory of DiMarco et al (1991) gives the velocity spectrum for the mean wind speed  $U$  as

$$S_v(\omega) = CU^5\omega^2k^{-2}(LU^{-3}\omega^4 - \rho' hU\omega^2 + \rho gU - \rho U^2\omega)^{-2}, \quad (46)$$

where  $C$  is a constant incorporating several measurable parameters. The total variance is proportional to  $U^3$  when  $U$  is small, but it increases as  $U^{11}$  as  $U$  nears critical. Good agreement has been found with tiltmeter data from a frozen lake (DiMarco et al 1991), and with Arctic data (Dugan et al 1992). However, the dispersion relation for the motions is yet to be confirmed as the Taylor condition  $\omega = Uk$ .

While motions due to this mechanism are highly constrained on the high frequency side because of the steep roll off ( $\omega^{-8}$ ), the energy is white at lower frequencies, and it easily fills the spectral gap between the internal waves and swell (Figure 18). At these lower frequencies, motions may be either wind-induced or due to internal waves, depending upon the specific local oceanographic and meteorological conditions.

At supercritical wind speeds, waves are generated resonantly [cf Phillips (1957) for ice-free water] at two frequencies. The horizontal line in Figure 19, which crosses the dispersion curve at two points, represents the locus of forcing for  $U = 30 \text{ m s}^{-1}$ . The higher frequency crossing is a function of the flexural rigidity  $L$  and hence the ice thickness. Because the equation of motion for the ice plate is forced at frequencies corresponding to the free wave speeds at these points, resonances occur there. The waves that are generated are expected to be quite large on thinner ice and they can propagate some small distance into the surrounding, thicker, multi-year floes (Dugan et al 1992). The waves presumably could get quite large on thicker floes if the wind speed were very high. This supercritical mechanism has not yet been fully validated with field data.

*Motions due to turbulence in the water* In theory a similar mechanism must occur for turbulence in the water boundary layer below the ice, but because the flow speed past the ice is slow ( $\sim 0.1 \text{ m s}^{-1}$ ) the mechanism is always subcritical. The ice velocity variance varies as  $U^3$ , just as above, and a modeled value of the spectrum is provided in curve D of Figure 18. For  $U > 0.3 \text{ m s}^{-1}$  the level shown in the figure is not significantly below

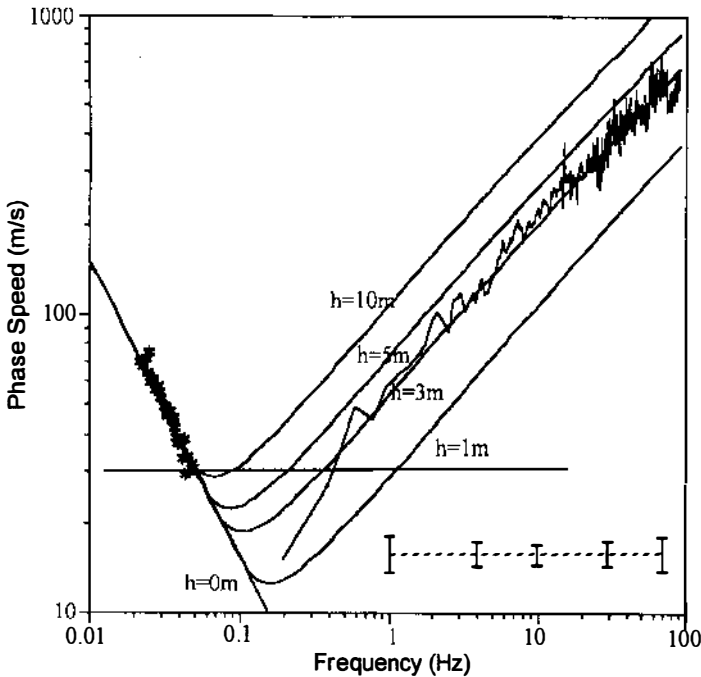


Figure 19 Theoretical dispersion relations for flexural-gravity waves compared with measurements. The several lines represent ice of the thickness as marked, while the effective elastic modulus is for nominal multi-year sea ice. (Redrawn from Dugan et al 1992.) Horizontal line A is the locus of wind turbulent forcing  $f$  for a mean wind speed of  $30 \text{ m s}^{-1}$ .

the level of the measured ice motions in the spectral gap between internal waves and swell.

I. Dyer (personal communication) speculates that quasi-static ice motions may be caused by lateral fluctuations in the forces on ice keels due to vortex shedding in the flow. Expected frequencies would be largest on the plate very close to the keels, but are generally low. The characteristic length  $l$  ( $\sim$ tens of meters for multi-year ice) determines the radius of influence.

There is no direct evidence to date that turbulence in the water causes measurable ice motions. Such motions would have a signature at low frequencies during periods when water speed past the floe is rapid but little wind is present.

**Floe-floe interactions** The ice cover in the interior of the Arctic Ocean does not move as a single ice unit. Local regions experience periods of dilation, when the ice opens up leads that refreeze very rapidly in the winter, and compression, when thinner (and sometimes thicker) ice is

broken up and rafted into layers or piled into pressure ridges and rubble fields. The resulting fracture and grinding of the ice is thought to account for much of the noise in the Arctic Ocean (Pritchard 1984, Makris & Dyer 1986). Activity in any particular region typically occurs on the order of hours, and the noise level over quiet periods may be more than four decades of power greater.

If ridging activity occurs on the margins of the instrumented floe, then the vertical motions are high between 0.2 and 10 Hz (curve E in Figure 18)—presumably because ridging has a strong flexural component—and they propagate across the floe as flexural waves, as shown by their dispersion relation plotted in Figure 19 (Dugan et al 1992). Although these waves are coupled to the ice-water-air interface, much acoustic energy also propagates into the water, generated by the fracturing process and the grinding of one ice block on another. In this situation, high-speed ( $1\text{--}3\text{ km s}^{-1}$ ) acoustic modes that propagate along the ice surface are overwhelmed by the high flexural energies generated simultaneously and acoustic waves are not apparent in the data. If, on the other hand, fracturing occurs only on floes removed from the instrumented floe, the motions in the band below 20 Hz or so are much reduced, while those at higher frequencies are energized. Only by establishing the dispersion relation can these waves be identified unequivocally.

Bogorodskiy & Smirnov (1982) have published interesting observations of what they call “relaxation self-excited oscillations” in both Arctic and Antarctic ice fields. These are high Q, SH-elastic motions (shear, horizontal polarization) having center frequencies near 1–2 Hz with durations of several minutes or longer and speeds of order  $1\text{--}3\text{ km s}^{-1}$ . It is postulated that the generation mechanism is slippage of one floe past another while under simultaneous compression and shear, and the term “stick-slip,” found in the fracture mechanics literature, is used by the AARI group. Czipott & Podney (1989) present time series that are similar, though somewhat lower in frequency at about 0.3 Hz, and have hypothesized that the motions were due to either a bobbing or rocking motion. This is difficult to imagine for a consolidated floe, so the mechanism for these as well as the AARI observations remains to be fully described and modeled.

*Miscellaneous events* Energetic flexural-gravity waves also have been observed to be generated by iceberg calving events in the Antarctic (Smirnov & Lin'kov 1967).

#### 4. CONCLUSIONS AND FUTURE WORK

Despite rapid advances in our understanding of wave-ice interaction processes in the past two decades, this review identifies a number of areas

where our knowledge is incomplete and further research is desirable. These revolve around the areas of developing theory further where it is inadequate; carrying out new measurements; and developing new uses for wave-ice interaction as a tool for understanding ice mechanics.

Helpful new theoretical developments include:

1. Developing a fully three-dimensional model for the motion and bending of a solitary ice floe that can be synthesized into MIZ scattering theory to model the passage of directional wave spectra.
2. Determining how wind-wave generation and wave attenuation balance in a diffuse ice field.
3. Applying novel rheological theories to various forms of sea ice acted upon by waves.
4. Determining how wave radiation pressure molds the ice edge profile.
5. Establishing how waves (particularly in the Antarctic) influence the large-scale dynamics, rheology, and thermodynamics of the ice cover.
6. Determining an ideal equilibrium floe size distribution as a function of distance of penetration, ice thickness, and incident wave spectrum.
7. Ascertaining the effect of ice thickness variability (e.g. ridging) on wave propagation and attenuation.

New observations required include:

1. Careful directional observations of short period (1–3 s), high Q, wave propagation in relation to nearby concurrent ice deformation processes.
2. Observations to determine whether there are circumstances in which either atmospheric or oceanic boundary layer turbulence is the dominant source of oscillatory motion in continuous ice sheets at low frequencies, and to validate unequivocally the supercritical mechanism for high-wind speed generation of large motions.
3. The measurement of the complete body and flexural response of an isolated floe to a known wave field.
4. Measurements of wave-induced floe collisions to determine whether they are inelastic.
5. Concurrent measurements of directional wave spectra in the MIZ and SAR retrievals, to establish wave imaging mechanisms.
6. Measurement of the failure strain of ice floes in flexure, by instrumenting floes near the ice edge that break up.

New applications suggested include:

1. The use of basin-wide swell attenuation as a means of monitoring mean ice thickness or some other distance-averaged material property of the Arctic pack.

2. Development of unmanned tiltmeter systems, transmitting spectral parameters by satellite, for monitoring wave activity in the central Arctic.
3. Development of an MIZ ambient noise model from knowledge of incident sea state alone.

The subject of wave-ice interaction still offers fascinating challenges to mathematicians, physicists, and engineers, and may offer a harvest of valuable applications that can improve our knowledge of sea ice mechanics and oceanographic processes in the polar seas.

#### ACKNOWLEDGMENTS

The authors are grateful to the Arctic Program of the U.S. Office of Naval Research, which has supported a number of the measurements and analyses under discussion. They also acknowledge the continued support of the U.K. Natural Environment Research Council, the Defence Research Agency (U.K.), the University of Otago (N.Z.), the U.S. National Aeronautics and Space Administration, and the N.Z. Foundation for Research, Science, and Technology. Progress in this area has resulted from interactions with a number of colleagues, including Hayley Shen of Clarkson University, Victor Smirnov of the Arctic and Antarctic Research Institute, Steve Ackley and Terry Tucker of the U.S. Army Cold Regions Research and Engineering Laboratory, and Willy Weeks of the University of Alaska.

The authors of this review are members of the I.A.P.S.O. (International Association for the Physical Sciences of the Ocean) Working Group on Wave-Ice Interaction under the Chairmanship of V.A.S. The support of I.A.P.S.O. is gratefully acknowledged.

**Any *Annual Review* chapter, as well as any article cited in an *Annual Review* chapter, may be purchased from the Annual Reviews Preprints and Reprints service.  
1-800-347-8007; 415-259-5017; email: arpr@class.org**

#### Literature Cited

- Alpers WR, Ross DB, Rufenach CL. 1981. On the detectability of ocean surface waves by real and synthetic aperture radar. *J. Geophys. Res.* 86(C7): 6481-98
- Armstrong TE, Roberts BB, Swithinbank C. 1973. *Illustrated Glossary of Snow and Ice*. Cambridge, UK: Scott Polar Res. Inst. Spec. Publ. 4. 2nd. ed. 60 pp.
- Bates HF, Shapiro LH. 1980. Long-period gravity waves in ice-covered sea. *J. Geophys. Res.* 85(C2): 1095-100
- Beal RC. 1987. Measuring ocean waves from space. *Proc. Symp. at APL/JHU, April 1986, Johns Hopkins APL, Tech. Digest* 8(1), 147 pp.
- Bogorodskiy VV, Smirnov VN. 1982. Relaxation processes in Arctic ice fields. *Dokl. Akad. Nauk SSSR* 250: 24-26
- Bratchie IL. 1984. *Modelling sea ice floe fields*. PhD thesis. Univ. Cambridge, UK. 236 pp.
- Buck BM, Wilson JH. 1986. Nearfield noise measurements from an Arctic pressure ridge. *J. Acoust. Soc. Am.* 80: 256-64

- Budden KG. 1988. *The Propagation of Radio Waves*. New York: Cambridge Univ. Press. 669 pp.
- Carsey F, Digby-Argus S, Collins M, Holt B, Livingstone C, Tang C. 1989. Overview of LIMEX'87 ice observations. *IEEE J. Geosci. Remote Sensing* 27: 468–82
- Carsey F, Holt B, Martin S, McNutt L, Rothrock D, et al. 1986. Weddell-Scotia sea marginal ice zone observations from space, October, 1984. *J. Geophys. Res.* 91(C3): 3920–24
- Clarke AJ. 1978. On wind-driven quasi-geostrophic water movement at fast ice edges. *Deep Sea Res.* 25: 41–51
- Crocker GB, Wadhams P. 1988. Observations of wind-generated waves in Antarctic fast ice. *J. Phys. Oceanogr.* 93: 1292–99
- Czipott PV, Podney WN. 1989. *Measurements of fluctuations in tilt of the Arctic ice at the CEAREX oceanography camp: experimental review, data catalog, and preliminary results*. Tech. Rep. PD-LJ-89-369R, Physical Dynamics Inc., La Jolla, CA
- Czipott PV, Podney WN, Levine MD, Paulsen CA, Williams R. 1990. *Ice flexure forced by an internal wave packet in the Arctic Ocean*. Presented at AGU Ocean Sci. Meet., New Orleans
- Davys JW, Hosking RJ, Sneyd AD. 1985. Waves due to a steadily moving source on a floating ice plate. *J. Fluid Mech.* 158: 269–87
- Diachok OI, Winokur RS. 1973. Spatial variability of underwater ambient noise at the Arctic ice-water boundary. *J. Acoust. Soc. Am.* 55: 750–53
- DiMarco RL, Dugan JP, Martin WW. 1991. Ice motions forced by boundary layer turbulence. *J. Geophys. Res.* 96(C6): 10,617–24
- Dugan JP, DiMarco RL, Martin, WW. 1992. Low frequency vibrational motion of arctic pack ice. *J. Geophys. Res.* 97(C4): 5381–88
- Dugan JP, Morris WM, Okawa BS. 1986. Horizontal wavenumber distribution of potential energy in the ocean. *J. Geophys. Res.* 91(C1): 12,993–3000
- Dyer I. 1983. The song of sea ice and other ocean melodies. In *Arctic Technology and Policy*, ed. I Dyer, C Chrysosostomidis, pp. 11–37. New York: Hemisphere
- Evans DV, Davies TV. 1968. *Wave-ice interaction*. Rep. 1313, Davidson Lab., Stevens Inst. Technol., Hoboken, NJ
- Ewing M, Cray AP. 1934. Propagation of elastic waves in ice, II. *Physics* 5: 181–84
- Ewing M, Cray AP, Thorne AM. 1934. Propagation of elastic waves in ice, I. *Physics* 5: 165–68
- Fox C. 1992. Large amplitude sea/ice coupling. In *Advances in Ice Technology Proc. 2nd Int. Conf. on Ice Tech.*, ed. TKS Murthy, WM Sackinger, P Wadhams, pp. 293–304. Boston: Comp. Mech. 365 pp.
- Fox C, Squire VA. 1990. Reflection and transmission characteristics at the edge of shore fast sea ice. *J. Geophys. Res.* 95(C7): 11,629–39
- Fox C, Squire VA. 1991a. Coupling between an ocean and an ice shelf. *Ann. Glaciol.* 15: 101–8
- Fox C, Squire VA. 1991b. Strain in shore fast ice due to incoming ocean waves and swell. *J. Geophys. Res.* 96(C3): 4531–47
- Fox C, Squire VA. 1994. On the oblique reflexion and transmission of ocean waves from shore fast sea ice. *Phil. Trans. R. Soc. A* 347(1682): 185–218
- Frank W. 1967. *Oscillation of cylinders in or below the free surface of deep fluids*. Naval Ship Res. and Develop. Centre, Hydro-mechanics Lab., Res. and Develop. Rep. 2375
- Fu LL, Holt B. 1982. *Seasat view oceans and sea ice with synthetic aperture radar*. JPL Publ. 81-120, Pasadena, CA. 200 pp.
- Gammelsrød T, Mork M, Roed LP. 1975. Upwelling possibilities at an ice-edge, homogeneous model. *Mar. Sci. Comm.* 1: 115–45
- Ganton JH, Milne AR. 1965. Temperature- and wind-dependent ambient noise under midwinter pack ice. *J. Acoust. Soc. Am.* 38: 406–11
- Gao L. 1992. *Ice floe collisions under wave action in the marginal ice zone*. M. Eng. thesis. Memorial Univ. Newfoundland, St. John's. 52 pp.
- Goodman DJ, Wadhams P, Squire VA. 1980. The flexural response of a tabular ice island to ocean swell. *Ann. Glaciol.* 1: 23–27
- Greene CR, Buck BM. 1964. Arctic ocean ambient noise. *J. Acoust. Soc. Am.* 36: 1218–20
- Greenhill AG. 1887. Wave motion in hydrodynamics. *Am. J. Math.* 9: 62–112
- Greenhill AG. 1916. Skating on thin ice. *Phil. Mag.* 31: 1–22
- Guest PS, Davidson KL. 1991. The aerodynamic roughness of different types of sea ice. *J. Geophys. Res.* 96(C3): 4709–21
- Hakkinen S. 1986. Coupled ice-ocean dynamics in the marginal ice zones: upwelling/downwelling and eddy generation. *J. Geophys. Res.* 91(C1): 819–32
- Hakkinen S. 1987. Upwelling at the ice edge: a mechanism for deep water formation? *J. Geophys. Res.* 92(C5): 5031–34
- Hasselmann K, Raney RK, Plant WJ, Alpers W, Shuchman RA, et al. 1985. Theory of synthetic aperture radar ocean imaging: a

- MARSEN view. *J. Geophys. Res.* 90(C3): 4659–86
- Hendrickson JA, Webb LM. 1963. *Theoretical investigation of semi-infinite ice floes in water of infinite depth*. Rep. NBy-32225, Natl. Engng. Sci. Co., Pasadena, CA
- Hunkins K. 1962. Waves on the Arctic Ocean. *J. Geophys. Res.* 67(6): 2477–89
- Ikeda M. 1985. A coupled ice-ocean model of a wind-driven coastal flow. *J. Geophys. Res.* 90(C5): 9119–28
- Ikeda M. 1989. A coupled ice-ocean mixed layer model of the marginal ice zone responding to wind forcing. *J. Geophys. Res.* 94(C7): 9699–709
- Johannessen OM, Sagen H, Sandven S, Starke KV, Payne SS, Engelsen I. 1990. *MIZEX 87: Ambient sound in the marginal ice zone*. Nansen Remote Sensing Centre Tech. Rep. No. 32
- Keller JB, Weitz M. 1953. Reflection and transmission coefficients for waves entering or leaving an icefield. *Commun. Pure Appl. Math.* 6(3): 415–17
- Kobayashi N., Frankenstein S. 1987. Wave drift force on ice floe. *J. Waterway, Port, Coastal, Ocean Eng.* 113: 476–92
- Lee CM. 1976. Motion characteristics of floating bodies. *J. Ship Res.* 20(4): 181–89
- Levine MD, Paulson CA, Morison JH. 1985. Internal waves in the Arctic Ocean: comparison with lower-latitude observations. *J. Phys. Oceanogr.* 15: 800–9
- Levine MD, Paulson CA, Morison JH. 1987. Observations of internal gravity waves under the Arctic pack ice. *J. Geophys. Res.* 92(C1): 779–82
- Liu AK, Hakkinen S, Peng CY. 1993. Wave effects in ocean-ice interaction in the marginal ice zone. *J. Geophys. Res.* 98(C6): 10,025–36
- Liu AK, Holt B, Vachon PW. 1991a. Wave propagation in the marginal ice zone: model predictions and comparisons with buoy and SAR data. *J. Geophys. Res.* 96(C3): 4605–21
- Liu AK, Mollo-Christensen E. 1988. Wave propagation in a solid ice pack. *J. Phys. Oceanogr.* 18: 1702–12
- Liu AK, Vachon PW, Peng CY. 1991b. Observation of wave refraction at an ice edge by SAR. *J. Geophys. Res.* 96(C3): 4803–8
- Liu AK, Vachon PW, Peng CY, Bhogal AS. 1992. Wave attenuation in the marginal ice zone during LIMEX. *Atmos. Ocean* 30(2): 192–206
- Longuet-Higgins MS. 1977. The mean forces exerted by waves on floating or submerged bodies with applications to sand bars and wave power machines. *Proc. R. Soc. A* 352: 463–80
- Lu Q-M, Larsen J, Tryde P. 1989. On the role of ice interaction due to floe collisions in marginal ice zone dynamics. *J. Geophys. Res.* 94(C10): 14525–37
- Lygre A, Krogstad HE. 1986. Maximum entropy estimation of the directional distribution of ocean wave spectra. *J. Phys. Oceanogr.* 16(12): 2052–60
- Lyzenga DR, Shuchman RA, Lyden LD, Rufenach CL. 1985. SAR imaging of wave in water and ice: evidence for velocity bunching. *J. Geophys. Res.* 90(C1): 1031–36
- Makris NC, Dyer I. 1986. Environmental correlates of pack ice noise. *J. Acoust. Soc. Am.* 79: 1434–40
- Makris NC, Dyer I. 1991. Environmental correlates of Arctic ice-edge noise. *J. Acoust. Soc. Am.* 90(6): 3288–98
- Martin S, Becker P. 1987. High-frequency ice floe collisions in the Greenland Sea during the 1984 Marginal Ice Zone Experiment. *J. Geophys. Res.* 92(C7): 7071–84
- Martin S, Becker P. 1988. Ice floe collisions and relation to ice deformation in the Bering Sea. *J. Geophys. Res.* 93(C2): 1303–15
- Martin S, Drucker R. 1991. Observations of short-period ice floe accelerations during leg II of the Polarbjørn drift. *J. Geophys. Res.* 96(C6): 10,567–80
- Martin S, Kauffman P. 1981. A field and laboratory study of wave damping by grease ice. *J. Glaciol.* 27(96): 283–313
- Martin S, Kauffman P, Parkinson C. 1983. The movement and decay of ice edge bands in the winter Bering Sea. *J. Geophys. Res.* 88(C5): 2803–12
- McKenna RF, Crocker GB. 1990. Wave energy and floe collisions in marginal ice zones. In *Ice Technology for Polar Operations, Proc. 2nd Int. Conf. on Ice Tech.*, ed. TKS Murthy, JG Paren, WM Sackinger, P Wadhams, pp. 33–45. Boston: Comp. Mech. 426 pp.
- McKenna RF, Crocker GB. 1992. Ice floe collisions interpreted from accelerometer data during LIMEX 1989. *Atmos.-Ocean* 30(2): 246–69
- Meylan M, Squire VA. 1993a. A model for the motion and bending of an ice floe in ocean waves. *Proc. 3rd Int. Offshore and Polar Eng. Conf.*, ed. JS Chung, BJ Natvig, BM Das, Y-C Li, Vol II, pp. 718–23. Golden, Colo.: Int. Soc. Offshore Polar Eng.
- Meylan M, Squire VA. 1993b. A model for the motion and bending of an ice floe in ocean waves. *Int. J. Offshore Polar Eng.* 3(4): 322–23.
- Meylan M, Squire VA. 1993c. Finite-floe wave reflection and transmission coefficients from a semi-infinite model. *J. Geophys. Res.* 98(C7): 12,537–42

- Meylan M, Squire VA. 1994a. The response of ice floes to ocean waves. *J. Geophys. Res.* 99(C1): 891–900
- Meylan M, Squire VA. 1994b. Changes to ocean wave spectra in a marginal ice zone 1. *Proc. 4th Int. Offshore and Polar Eng. Conf.*, ed. JS Chung, BJ Natvig, BM Das, Vol. III, pp. 136–41. Golden, Colo.: Int. Soc. Offshore and Polar Eng.
- Milne AR. 1972. Thermal tension cracking in sea ice: a source of underwater noise. *J. Geophys. Res.* 77(12): 2177–92
- Milne AR. 1974. Wind noise under winter ice fields. *J. Geophys. Res.* 79(6): 803–9
- Munk WH, Snodgrass FE, Tucker MJ. 1959. Spectra of low-frequency ocean waves. *Bull. Scripps Inst. Oceanogr.* 7: 283–362
- Niebauer HJ. 1982. Wind and melt driven circulation in a marginal ice edge frontal system: a numerical model. *Cont. Shelf Res.* 1: 49–98
- Nikolayev SG. 1973. Experiment in organizing oceanographic investigations of the ice-edge zone of the Chukchi Sea. *Prob. Arktikii Antarkt.* 42: 31–36
- Oliver J, Crary AP, Cotell R. 1954. Elastic waves in Arctic pack ice. *Eos, Trans. Am. Geophys. Union* 35: 282–92
- Peters AS. 1950. The effect of a floating mat on water waves. *Commun. Pure Appl. Math.* 3: 319–54
- Phillips OM. 1957. On the generation of waves by the turbulent wind. *J. Fluid Mech.* 2: 417–45
- Phillips OM. 1977. *The Dynamics of the Upper Ocean*, pp. 139–59. New York: Cambridge Univ. Press. 2nd ed. 336 pp.
- Pinkel R. 1975. Upper ocean internal wave observations from FLIP. *J. Geophys. Res.* 80(27): 3892–910
- Press F, Crary AP, Oliver J, Katz S. 1951. Air-coupled flexural waves in floating ice. *Eos, Trans. Am. Geophys. Union* 32: 166–72
- Press F, Ewing M. 1951. Propagation of elastic waves in a floating ice sheet. *Eos, Trans. Am. Geophys. Union* 32: 673–78
- Pritchard RS. 1984. Arctic ocean background noise cause by ridging of sea ice. *J. Acoust. Soc. Am.* 75: 419–27
- Robin G de Q. 1963. Wave propagation through fields of pack ice. *Phil. Trans. R. Soc. A* 255: 313–39
- Robinson NJ, Palmer SC. 1990. A modal analysis of a rectangular plate floating on an incompressible liquid. *J. Sound Vib.* 42: 453–60
- Røed LP, O'Brien JJ. 1983. A coupled ice-ocean model of upwelling in the marginal ice zone. *J. Geophys. Res.* 88(C5): 2863–72
- Roethlisberger H. 1972. Surface waves and waves in thin floating ice. *Cold Reg. Res. Eng. Lab. Monogr.* II-A2a: 105–9
- Rottier P. 1991. *Wave-ice interaction in the marginal ice zone and the generation of ocean noise*. PhD thesis. Univ. Cambridge, UK. 250 pp.
- Rottier PJ. 1992. Floe pair interaction event rates in the marginal ice zone. *J. Geophys. Res.* 97(C6): 9391–400
- Rottier PJ, Squire VA. 1993. Collision events between adjacent ice floes driven by an ocean wavefield. *Proc. 3rd Int. Offshore and Polar Eng. Conf.*, ed. JS Chung, BJ Natvig, BM Das, Y-C Li, Vol II, pp. 747–51. Golden, Colo.: Int. Soc. Offshore Polar Eng.
- Rumer RR Jr, Crissmas RD, Wake A. 1979. *Ice transport in Great Lakes*. Water Resources and Environ. Eng. Res. Rep. 79-3, SUNY, Buffalo, NY. 275 pp.
- Shapiro A, Simpson LS. 1953. The effect of a broken icefield on water waves. *Trans. Am. Geophys. Union* 34(1): 36–42
- Shemdin OH. 1988. Tower ocean wave and radar dependence experiment: an overview. *J. Geophys. Res.* 93(11): 13829–36
- Shen HH, Ackley SF. 1991. A one-dimensional model of wave-induced ice-floe collisions. *Ann. Glaciol.* 15: 87–95
- Shen HH, Hibler WD III, Leppäranta M. 1987. The role of floe collisions in sea ice rheology. *J. Geophys. Res.* 92(C7): 7085–96
- Smirnov VN. 1972. Oscillations of the ice cover generated by internal waves of Arctic Ocean. *Dokl. Akad. Nauk SSSR* 206
- Smirnov VN, Lin'kov EM. 1967. On a source of high frequency seismic disturbances and flexural-gravity waves in the Antarctic. *Izv. Earth Phys.* 8: 542–54
- Squire VA. 1978. *Dynamics of ocean waves in a continuous sea ice cover*. PhD thesis. Univ. Cambridge, UK. 191 pp.
- Squire VA. 1981. *Numerical simulation of ice floes in waves*. SPRI Tech. Rep. 81-1, Scott Polar Res. Inst., Univ. Cambridge, UK. 57 pp.
- Squire VA. 1982. Numerical modelling of realistic ice floes in ocean waves. *Ann. Glaciol.* 4: 277–82
- Squire VA. 1983. Dynamics of ice floes in sea waves. *J. Soc. Underwater Tech.* 9(1): 20–26
- Squire VA. 1984a. Sea ice. *Sci. Prog. Oxford.* 69: 19–43
- Squire VA. 1984b. A theoretical, laboratory and field study of ice-coupled waves. *J. Geophys. Res.* 89(C5): 8069–79
- Squire VA. 1984c. On the critical angle for waves entering shore fast ice. *Cold Reg. Sci. Tech.* 10(1): 59–68
- Squire VA. 1984d. How waves break up inshore fast ice. *Polar Rec.* 22(138): 281–5
- Squire VA. 1986. Wind over ice: a mechanism for the generation of ice-coupled

- waves. In *Ice Technology, Proc. 1st Int. Conf.*, ed. TKS Murthy, JJ Connor, CA Brebbia, pp. 115–28. Berlin: Springer-Verlag. 594 pp.
- Squire VA. 1989. Super-critical reflection of ocean waves: a new factor in ice edge dynamics? *Ann. Glaciol.* 12: 157–61
- Squire VA. 1993a. The breakup of shore fast sea ice. *Cold Reg. Sci. Tech.* 21(3): 211–18
- Squire VA. 1993b. A comparison of the mass-loading and elastic-plate models of an ice field. *Cold Reg. Sci. Tech.* 21(3): 219–29
- Squire VA. 1993c. Ocean wave propagation in an ice field with varying concentration. *Proc. 3rd Int. Offshore and Polar Eng. Conf.*, ed. JS Chung, BJ Natvig, BM Das, Y-C Li, Vol II, pp. 724–29. Golden, Colo.: Int. Soc. Offshore Polar Eng.
- Squire VA, Allan AJ. 1980. Propagation of flexural gravity waves in sea ice. In *Sea Ice Processes and Models*, ed. RS Pritchard, pp. 327–38. Seattle: Univ. Wash. Press. 474 pp.
- Squire VA, Fox C. 1990. The wave structure in the seas off an ice edge. In *Ice Technology for Polar Operations, Proc. 2nd Int. Conf. on Ice Tech.*, ed. TKS Murthy, JG Paren, WM Sackinger, P Wadhams, pp. 21–32. Boston: Comp. Mech. 426 pp.
- Squire VA, Fox C. 1991. The role of incoming waves in ice edge dynamics. *Ann. Glaciol.* 15: 96–100
- Squire VA, Fox C. 1992. On ice-coupled waves: a comparison of data and theory. In *Advances in Ice Technology, Proc. 2nd Int. Conf. on Ice Tech.*, ed. TKS Murthy, WM Sackinger, P Wadhams, pp. 269–80. Boston: Comp. Mech. 365 pp.
- Squire VA, Martin S. 1980. *A field study of the physical properties, response to swell, and subsequent fracture of a single ice floe in the winter Bering Sea.* Univ. Wash. Sci. Rep. 18, Dept. Atmos. Sci. and Oceanogr.
- Squire VA, Meylan M. 1994. Changes to ocean wave spectra in a marginal ice zone 2. *Proc. 34th Int. Offshore and Polar Eng. Conf.*, ed. JS Chung, BJ Natvig, BM Das, Vol III, pp. 142–46. Golden, Colo.: Int. Soc. Offshore Polar Eng. In press
- Squire VA, Moore SC. 1980. Direct measurement of the attenuation of ocean waves by pack ice. *Nature, Lond.* 283(5745): 365–68
- Squire VA, Rottier P, Fox C. 1994. A first look at some wave-ice interaction data from McMurdo Sound, Antarctica. *Proc. 1st Int. Symp. Sea Ice.* Beijing, China. In press
- Tang CL, Ikeda M. 1989. Ice-edge upwelling off the Newfoundland coast during LIMEX. *Atmos. Ocean* 27: 658–81
- Wadhams P. 1972. Measurement of wave attenuation in pack ice by inverted echo sounding. In *Sea Ice*, ed. T Karlsson, pp. 255–60. Reykjavik: Nat. Res. Council. Iceland
- Wadhams P. 1973a. *The effect of a sea ice cover on ocean surface waves.* PhD thesis. Univ. Cambridge, UK. 223 pp.
- Wadhams P. 1973b. Attenuation of swell by sea ice. *J. Geophys. Res.* 78(18): 3552–63
- Wadhams P. 1975. Airborne laser profiling of swell in an open ice field. *J. Geophys. Res.* 80(33): 4520–28
- Wadhams P. 1978. Wave decay in the marginal ice zone measured from a submarine. *Deep Sea Res.* 25: 23–40
- Wadhams P. 1983. A mechanism for the formation of ice edge bands. *J. Geophys. Res.* 88(C5): 2813–18
- Wadhams P. 1986. The seasonal ice zone. In *The Geophysics of Sea Ice*, ed. N. Untersteiner, pp. 825–991. New York: Plenum
- Wadhams P, Holt B. 1991. Waves in frazil and pancake ice and their detection on Seasat SAR imagery. *J. Geophys. Res.* 96(C5): 8835–52
- Wadhams P, Kristensen M, Orheim O. 1983. The response of Antarctic icebergs to ocean waves. *J. Geophys. Res.* 88(C10): 6053–65
- Wadhams P, Squire VA, Ewing JA, Pascal RW. 1986. The effect of marginal ice zone on the directional wave spectrum of the ocean. *J. Phys. Oceanogr.* 16: 358–76
- Wadhams P, Squire VA, Goodman DJ, Cowan AM, Moore SC. 1988. The attenuation rates of ocean waves in the marginal ice zone. *J. Geophys. Res.* 93(C6): 6799–818
- Wadhams P, Squire VA, Liu A, Dugan J, Czipott P, et al. 1992. Workshop on wave-ice interaction. *Eos, Trans. Am. Geophys. Union* 73(35): 375–78
- Weber JE. 1987. Wave attenuation and wave drift in the marginal ice zone. *J. Phys. Oceanogr.* 17: 2351–61
- Weitz M, Keller JB. 1950. Reflection of water waves from floating ice in water of finite depth. *Commun. Pure Appl. Math.* 3(3): 305–18
- Williams RG, Davis NR, Moore SC. 1990. The Coordinated Eastern Arctic Experiment: SPRI sea-ice studies. *Polar Record* 26(158): 203–10
- Yang TC, Gellis GR, Votaw CW, Diachok OI. 1987. Acoustic properties of ice edge noise in the Greenland Sea. *J. Acoust. Soc. Am.* 82(3): 1034–38